63-2-3

DOC. NO.
NARF-62-16T
FZK-9-183-1



# ENERGY AND ANGULAR DISTRIBUTION EXPERIMENT

## Volume I: Angular Distribution of Reactor Radiation from Slabs and of Emergent Secondary Gamma Rays



USAF

NUCLEAR AEROSPACE RESEARCH FACILITY

operated by

GENERAL DYNAMICS | FORT WORTH

DOC. NO.
NARF-62-16T
FZK-9-183-1

DOC. NO.
NARF-62-16T
FZK-9-183-1

USAF

NUCLEAR AEROSPACE RESEARCH FACILITY

31 DECEMBER 1962

# ENERGY AND ANGULAR DISTRIBUTION EXPERIMENT

## Volume I: Angular Distribution of Reactor Radiation from Slabs and of Emergent Secondary Gamma Rays

G. T. WESTERN

CONTRACT
AF(657)-7201

SECTION II, TASK I, ITEM 6
OF FZM-2386

ISSUED BY THE
ENGINEERING
DEPARTMENT

GENERAL DYNAMICS | FORT WORTH

ABSTRACT

Radiation from the Aerospace Systems Test Reactor positioned within the Outside ASTR Tank was directed, with a narrow-beam slab geometry, onto test materials of 3% borated polyethylene and of lead. Measurements for polyethylene and lead, except as noted, were made of (1) the radiation source term; (2) the flux distribution of thermal and fast neutrons within the test materials; (3) the angular distribution of thermal- and epithermal-neutron flux, fast-neutron dose rate, and secondary gamma rays from the test materials; (4) the reflection of neutrons from borated polyethylene and from steel; (5) the angular distribution of fast-neutron and gamma-ray number-energy flux; and (6) the angular distribution of gamma-ray dose rate resulting from primary gamma rays scattering in and from the test materials. Data for items 1, 2, 3, and 4 are presented in Volume I of this report; data for items 5 and 6 will be published in Volume II.

## ACKNOWLEDGMENTS

The author wishes to express his appreciation to R. E. Beissner and H. G. Carter of the Nuclear Shielding Analysis Group for their many helpful suggestions which contributed significantly to the success of the experiment. Particular appreciation is expressed to R. E. Beissner for his contribution of Section II of this report.

The author wishes to acknowledge the invaluable contribution of the personnel from the Nuclear Shielding Experimental Group for their efficient performance of the experiment. Particular appreciation is expressed to B. O. McCauley who, as lead crew chief, directed the experimental setup and coordinated the efforts of personnel assigned to the experiment.

## REPORT SUMMARY

An experiment was performed for the purpose of obtaining information which would be of use in the development and verification of methods designed to predict the transport of nuclear radiation.

The experiment involved a narrow beam of neutrons and gamma rays from the Aerospace Shield Test Reactor incident to various thicknesses of 3% borated polyethylene slabs and lead slabs. The maximum test material thicknesses investigated were 15 and 6 inches for borated polyethylene and lead, respectively. Angular distributions of the radiation emerging from the test materials were determined for the slow-neutron flux, fast-neutron and gamma-ray dose rate, the secondary gamma-ray flux, and the angular distribution of fast-neutron and gamma-ray number-energy flux. Additional measurements were made to determine the reflection of fast and slow neutrons from 4-in.-thick slabs (each) of 3% borated polyethylene and steel.

The experimentally determined angular distributions of fast-neutron and gamma-ray dose rate obtained for each thickness of test material show two distinct contributions to the total distribution - scattered and uncollided. The foregoing indicates that theoretical methods designed to predict the transport of radiation through slabs should treat the uncollided and scattered fluxes as

two separate components. Of additional significance is the small thickness of polyethylene required for the scattered component to reach equilibrium and develop its asymptotic shape, equilibrium being reached for fast and epithermal neutrons at a thickness of 3 inches. For lead, the asymptotic behavior of the fast-neutron scattered component is closely approximated at a slab thickness of 4 inches.

Measurements of the reflection of neutrons from 4-in.-thick slabs show that the reflected fast-neutron dose rate is greater from steel than from polyethylene by a factor of 3. Further investigations of the reflection of radiation from shield materials as a function of material thickness should provide valuable information for the design of shielded compartments. Relative positions of hydrogenous and high-Z materials could considerably affect the contributions to total dose rate from the reflected and secondary gamma-ray components.

TABLE OF CONTENTS

TABLE OF CONTENTS (cont'd)

## LIST OF FIGURES

LIST OF FIGURES (cont'd)

LIST OF FIGURES (cont'd)

# I. INTRODUCTION

An experiment involving a narrow beam of radiation incident on test-material slabs of lead and of 3% borated linear polyethylene was performed at General Dynamics/Fort Worth (GD/FW). The experiment was designed to provide data on (1) the angular distribution of emergent neutron and gamma-ray number-energy flux and dose rate, (2) the distribution of neutron flux within the test materials, and (3) the angular distribution of emergent secondary gamma rays produced as a result of $(n_{th},\gamma)$ and $(n,n'\gamma)$ reactions within the test materials.

Extensive pre-planning and preliminary experimental investigations were made to evolve a good experimental narrow-beam geometry. These efforts were successful in that a well-defined beam of radiation was obtained and undesirable leakage and streaming of neutrons and gamma rays was effectively suppressed.

Upon completion of the planned experiment, additional data were obtained because of the well-defined narrow-beam geometry which had been evolved. These data were obtained on the reflection of neutrons from 4-in.-thick slabs of 3% borated polyethylene and of Type 304 steel.

Because of the quantity and variety of measurements, the experimental data are reported in two separate volumes. Volume I includes all experimental results except the spectral data involving the angular distribution of fast-neutron and gamma-ray number-energy flux. Volume II (Ref. 1) will report the neutron and gamma-ray spectral data.

## II. TECHNICAL DISCUSSION

The experimental method is based on a reciprocity theorem from transport theory. According to the theorem, and with reference to Figure 1, the energy-angular flux $F(x,\Theta,E)$ that is transmitted through a slab of thickness $x$ and that is due to an infinite plane source is equal to the surface integral of the flux $f(x,r,\Theta,E)$ penetrating an identical slab but due to an elementary (line-beam) source. That is,

$$F(x,\Theta,E) = 2\pi \int_0^{\infty} f(x,r,\Theta,E)\, r\, dr.$$

The flux received at $R,\Theta_o$ is

$$D(x,R,\Theta_o,E) = \int_{r=0}^{\infty} \int_{\phi=0}^{2\pi} (\ell^2)^{-1} f(x,r,\Theta,E) \cos\Theta \, r\, dr\, d\phi.$$

If, for a line-beam source, $r_{max}$ is the off-centerline distance beyond which the transmitted flux $f(x,r,\Theta,E)$ is negligible and $r_{max} \ll R$, then $\ell \cong R$, $\Theta \cong \Theta_o$, and

$$D(x,R,\Theta_o,E) \cong 2\pi\ (R^2)^{-1} \cos\Theta_o \int_{r=0}^{r_{max}} f(x,r,\Theta_o,E)\, r\, dr$$

or

$$D(x,R,\Theta_o,E) \cong (R^2)^{-1} \cos\Theta_o\, F(x,\Theta_o,E).$$

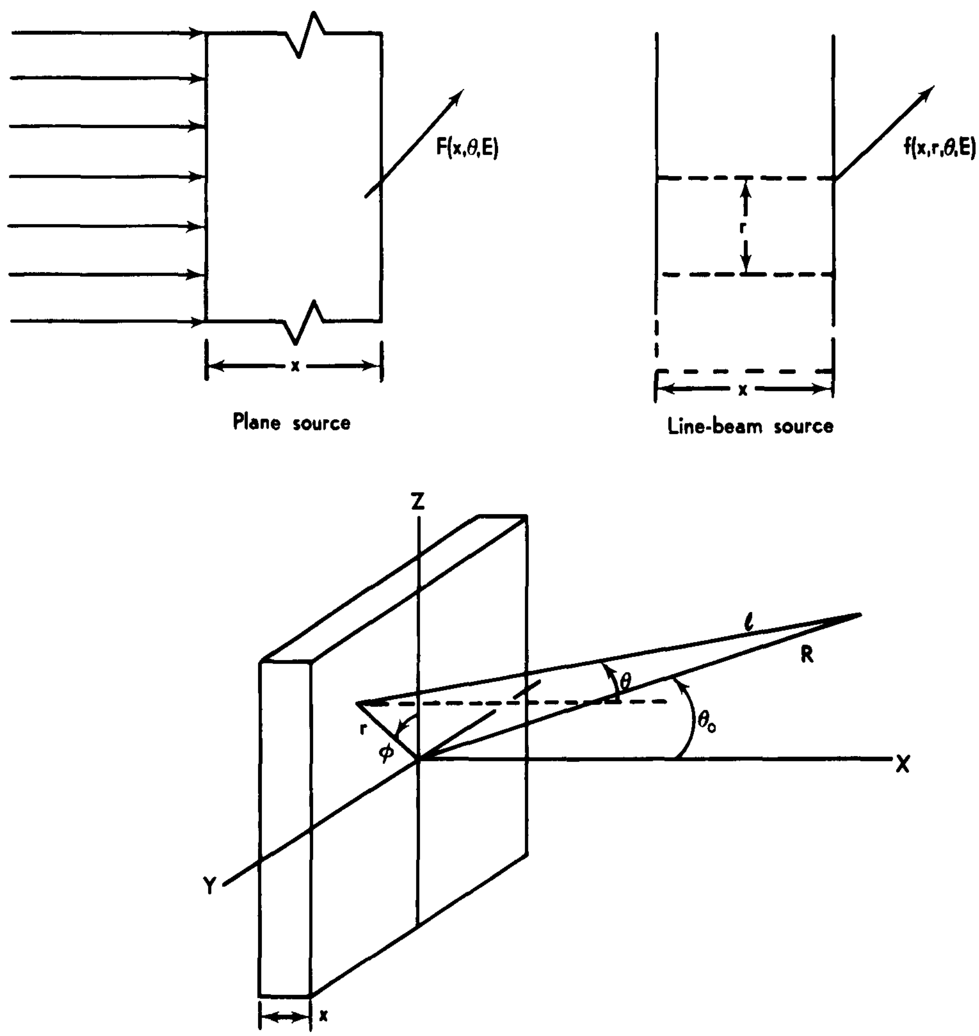


**Figure 1. Geometrical Considerations**

Therefore, data accumulated from a detector located at the coordinates R (constant) and $\theta_o$ (variable) may be related to the angular flux from an infinite plane source provided $r_{max} \ll R$. This means that virtually all of the flux transmitted through the slab must be confined to a circle on the slab surface whose radius is small compared to the slab-detector distance. The "important region" on the slab surface depends, of course, on the slab thickness and the incident-beam diameter. It was therefore important in designing the experiment to establish a beam of minimum diameter, commensurate with required intensity, and to make the slab area and slab-detector separation distance as large as possible.

For the experimental measurements to be of meaningful value, it was further required that (1) the undesirable components of radiation leakage and streaming be effectively suppressed, (2) the effects of source-collimator wall scattering and edge penetration be minimized for both neutrons and gamma rays, and (3) the contribution of secondary gamma rays produced within the source-collimator configuration be effectively attenuated prior to reaching the test material.

Preliminary experimental investigations, which are described in following sections, confirmed the fact that all of the foregoing requirements were satisfied.

## III. EXPERIMENTAL ARRANGEMENT

The Aerospace Systems Test Reactor (ASTR), described in Reference 2, was positioned within the Outside ASTR Tank (OAT) to serve as the source of radiation for the experiment. An external view of the OAT with its weather dome is shown in Figure 2. Shown in Figure 3 is the internal experimental geometry of the OAT, which remained constant throughout the experiment. The 4-in.-thick lead shield located between the ASTR and the void region was installed for the purpose of reducing the after-shutdown gamma-ray leakage and increasing the neutron-to-gamma ratio.

To prevent possible water leakage into the void region, air pressure of 8 psi was maintained within the void compartment, which consisted of an aluminum box of 1-in.-wall thickness and two air bags. As a means of determining that water was not in the void region, a system of radiation detectors was set up and monitored to detect any significant change in the neutron leakage through the OAT void.

Satisfactory performance of the experiment required that the geometry external to the OAT be flexible to the extent that the neutron-to-gamma ratio of the beam of radiation from the ASTR could be varied over a large range of values. The three experimental geometries used and the purpose for which each was intended are described in the following sections.


Figure 2. OAT Facility

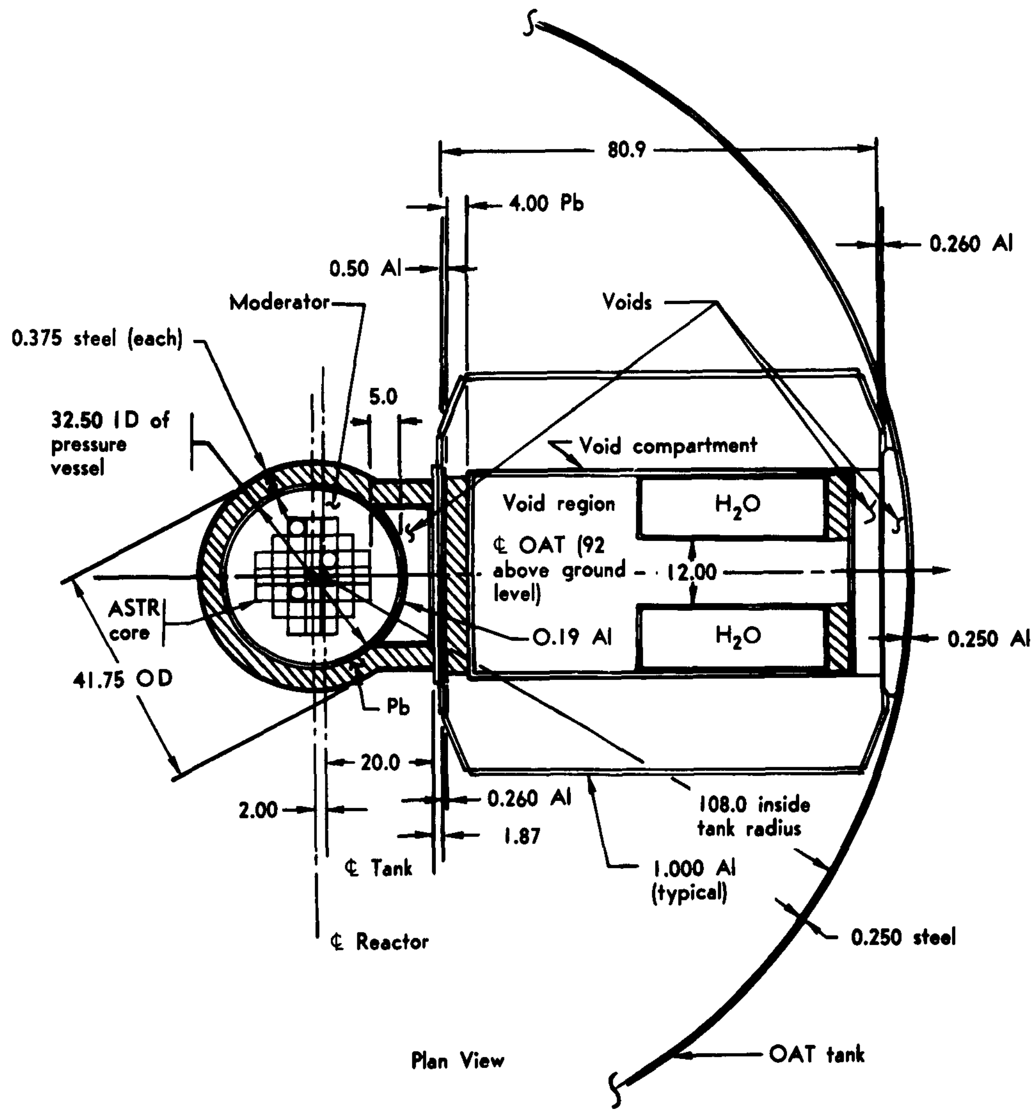


Notes: 1. OAT tank is filled with $H_2O$ except as noted
2. Drawn to scale
3. All dimensions in inches

**Figure 3. Internal Experimental Geometry of the OAT**

## 3.1 OAT Geometry I

Following a series of preliminary investigations, it was determined that the experimental arrangement shown in Figure 4 would provide a satisfactory narrow-beam geometry in that an infinite-slab condition could be closely approximated and, at the same time, radiation fluxes of sufficient intensity to obtain reliable data would be available. In constructing the concrete shield wall and the 6-in.-diam by 76-in.-long source collimator, no line-of-sight void regions, except the collimator opening, were allowed to exist between the ASTR and any detector position. The 1-in.-thick lead slab between the external source collimator and the OAT wall was inserted to increase the fast-neutron* to gamma dose-rate ratio to approximately 25; this was necessary in order to expose nuclear emulsion plates behind large thicknesses of polyethylene slabs without undue gamma fogging of the plates.

The test materials investigated were 3% borated linear polyethylene slabs made up of 1- by 48- by 72-in. sections and chemically pure lead slabs made up of 1- by 39- by 39-in. sections. The lead slabs were positioned normal to, and symmetrical about, the centerline of the source collimator, whereas the polyethylene slabs, positioned as shown in Figure 4, were symmetrical about the collimator centerline on three sides only. The position of the exit side of the slabs remained constant throughout the experiment. In addition, the window in the concrete wall into which the test material slabs were positioned was adjustable so that it was

*The fast-neutron dose rate was based on an RBE of 10.

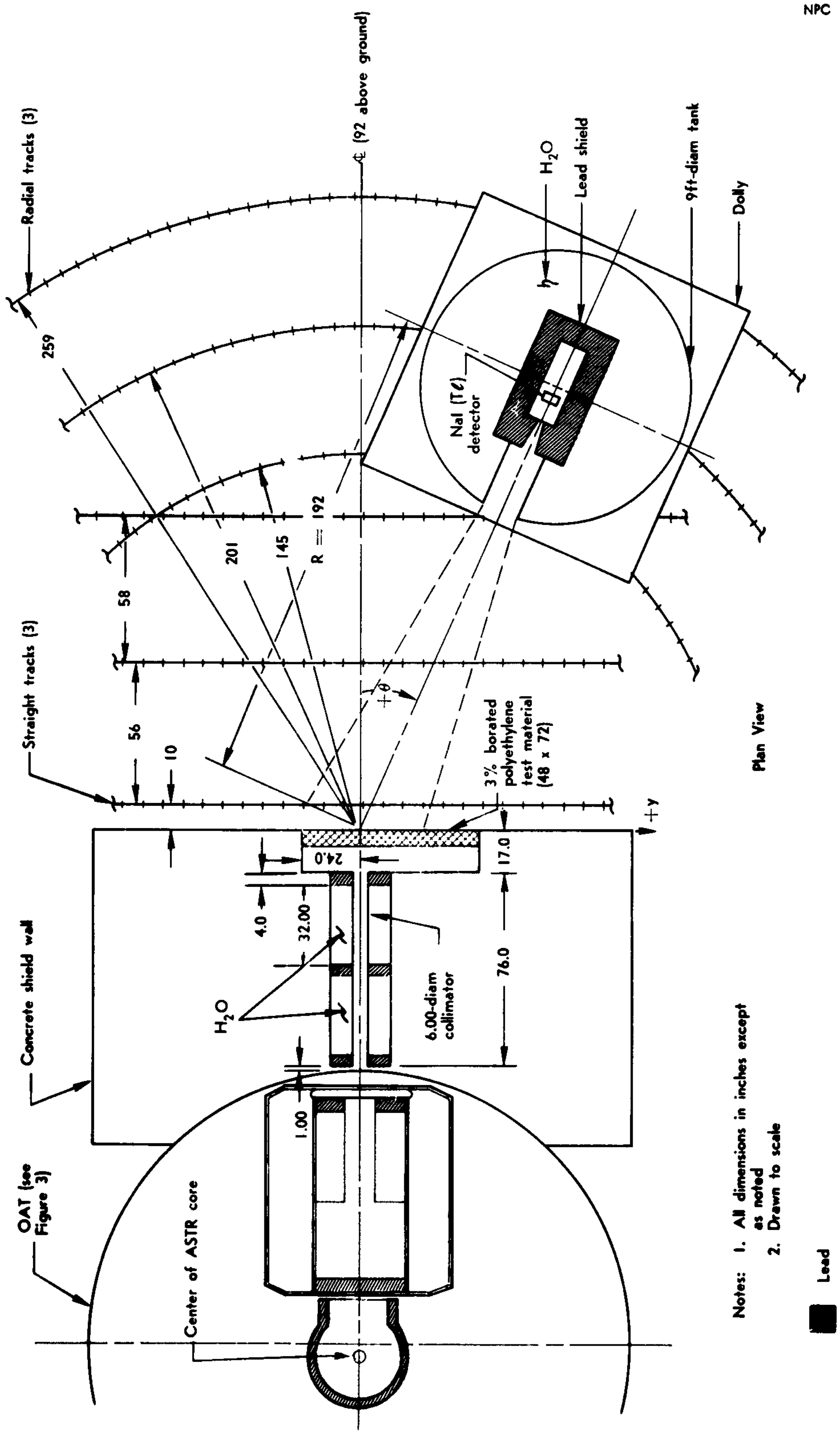


**Figure 4. OAT Geometry I: High Fast-Neutron-to-Gamma-Ray Ratio**

possible to keep the edges of the slabs, regardless of size, in contact with the concrete.

To obtain mapping data, a system of straight and circular tracks was installed. This is shown in Figure 5, a pictorial view of the geometry shown in Figure 4. The dolly, containing selected detectors positioned horizontal to the ground, was remotely positioned through the use of a closed-circuit television system. Also shown in Figure 5 is a 9-ft-diam by 9-ft-high tank into which is being positioned a lead shield containing the gamma-ray spectrometer. When the lead shield is in position, the tank is filled with water to reduce the flux of neutrons incident upon the shield. The complete assembly forms a collimator-shield system for the gamma-ray spectrometers used during the experiment. Shown in Figure 6 is a cross-sectional view of the collimator-shield system. Figure 7 defines the collimators used for 1- and 3-crystal gamma-ray spectrometers.

With the exception of gamma-ray spectral data, all data were accumulated by means of uncollimated detectors and uncollimated nuclear emulsion plates.

## 3.2 OAT Geometry II

That portion of the experiment wherein data on the angular distribution of gamma-ray dose rate and gamma-ray number-energy flux were obtained required that the production of secondary gamma rays within the test materials be effectively suppressed. To

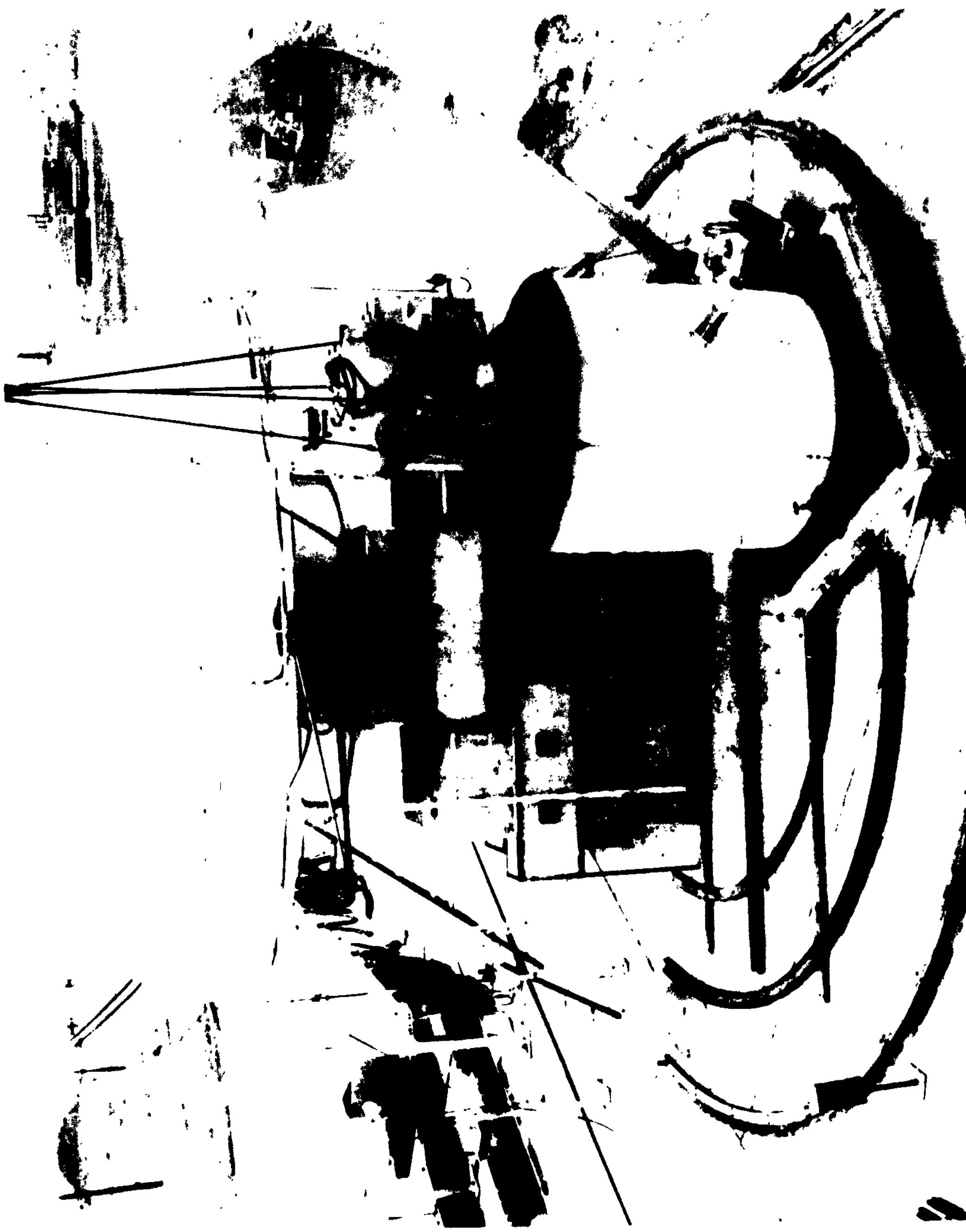

Figure 5. External View of Experimental Geometry

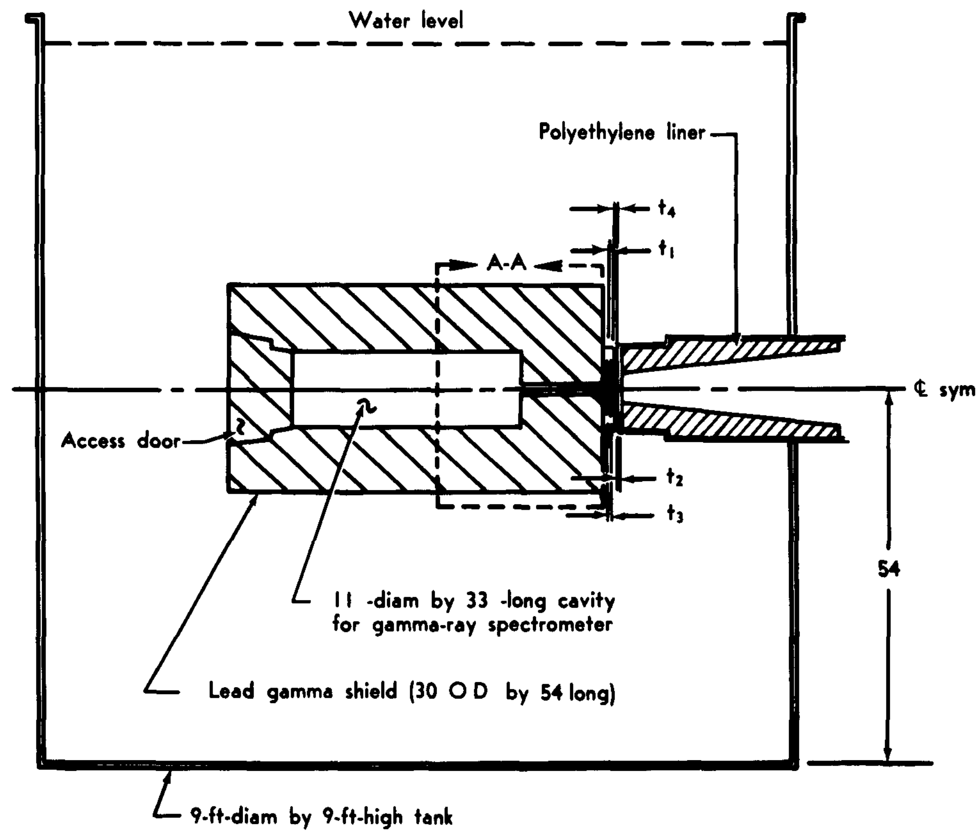


Note: $t_1 + t_2 = 0.32''$ aluminum

$t_3 + t_4 = 0.50''$ boroxy (35% $B_4C$ and 65% epoxy resin)

All dimensions in inches except as noted

Side Cross-Sectional View

**Figure 6. Collimator-Shield System for the Gamma-Ray Spectrometers**

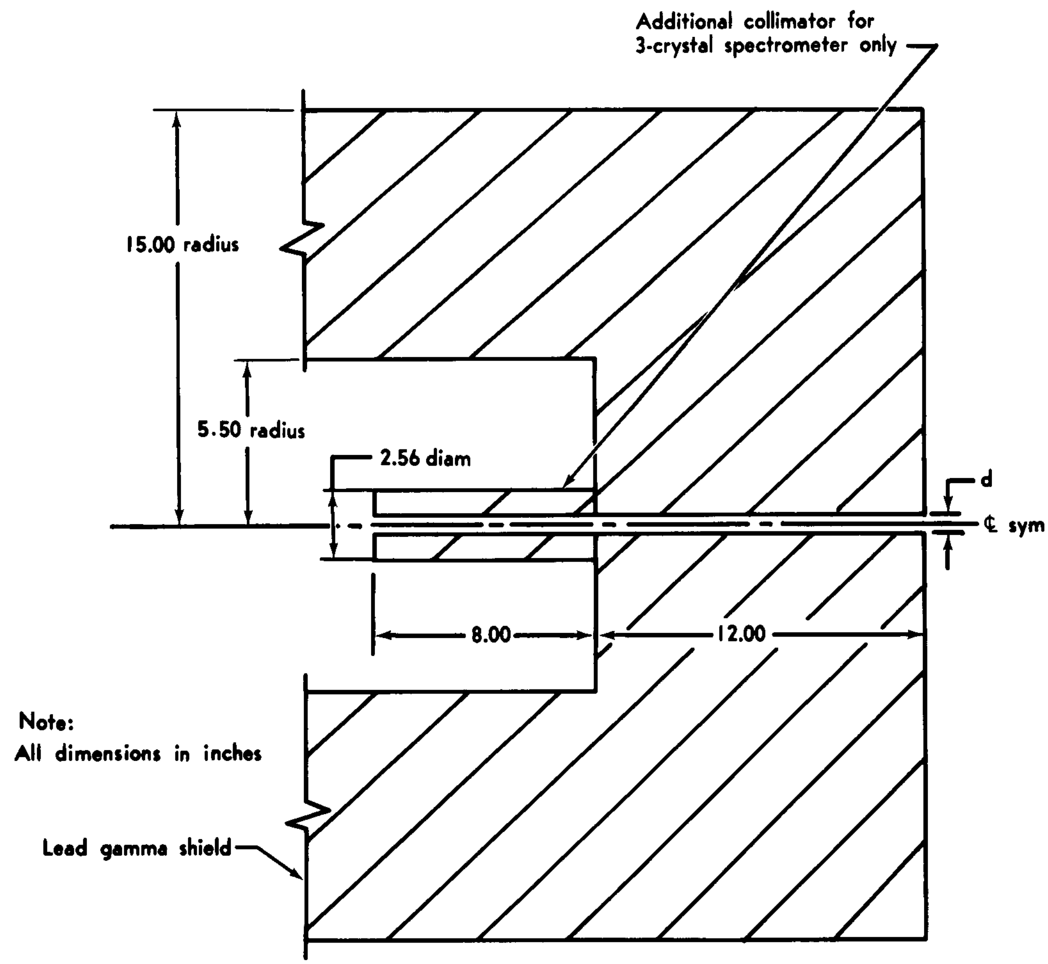


Note: Diameter, d = 1.60" for 5". diam x 4" long NaI spectrometer
d = 0.75" for 3-crystal anticoincidence
NaI spectrometer

View A-A of Figure 6

**Figure 7. Collimator Geometries**

accomplish this reduction in secondary gamma rays, a 5.88-in.-diam by 15-in.-long polyethylene plug was inserted into the 6-in.-diam source collimator (Fig. 4) at a point adjacent to the external wall of the OAT. Insertion of this plug reduced the fast-neutron to gamma-ray dose-rate ratio at the test sample position by a factor of 250 - i.e., the fast-neutron dose rate decreased by a factor of 1000 whereas the gamma-ray dose rate decreased by only a factor of 4. It was experimentally determined that, with this geometry, secondary gamma-ray production within the test sample was effectively suppressed.

### 3.3 OAT Geometry III

The geometry shown in Figure 8 was established to provide a means of accumulating data on the reflection of neutrons. Fast-neutron dose rates and relative neutron flux data, above and below the cadmium cutoff, were obtained as a function of y for values of h = 12 and 24 inches. All detectors were mounted vertical to the collimator centerline to prevent attenuation of the primary beam prior to reaching the test material.

The test-material slabs were suspended by two steel cables to minimize the mass of supporting structure. The 4-in.-thick, 3% borated polyethylene slab was made of the polyethylene slabs described in Section 3.1, whereas the steel slab was made of four 1- by 39- by 39-in. steel plates.

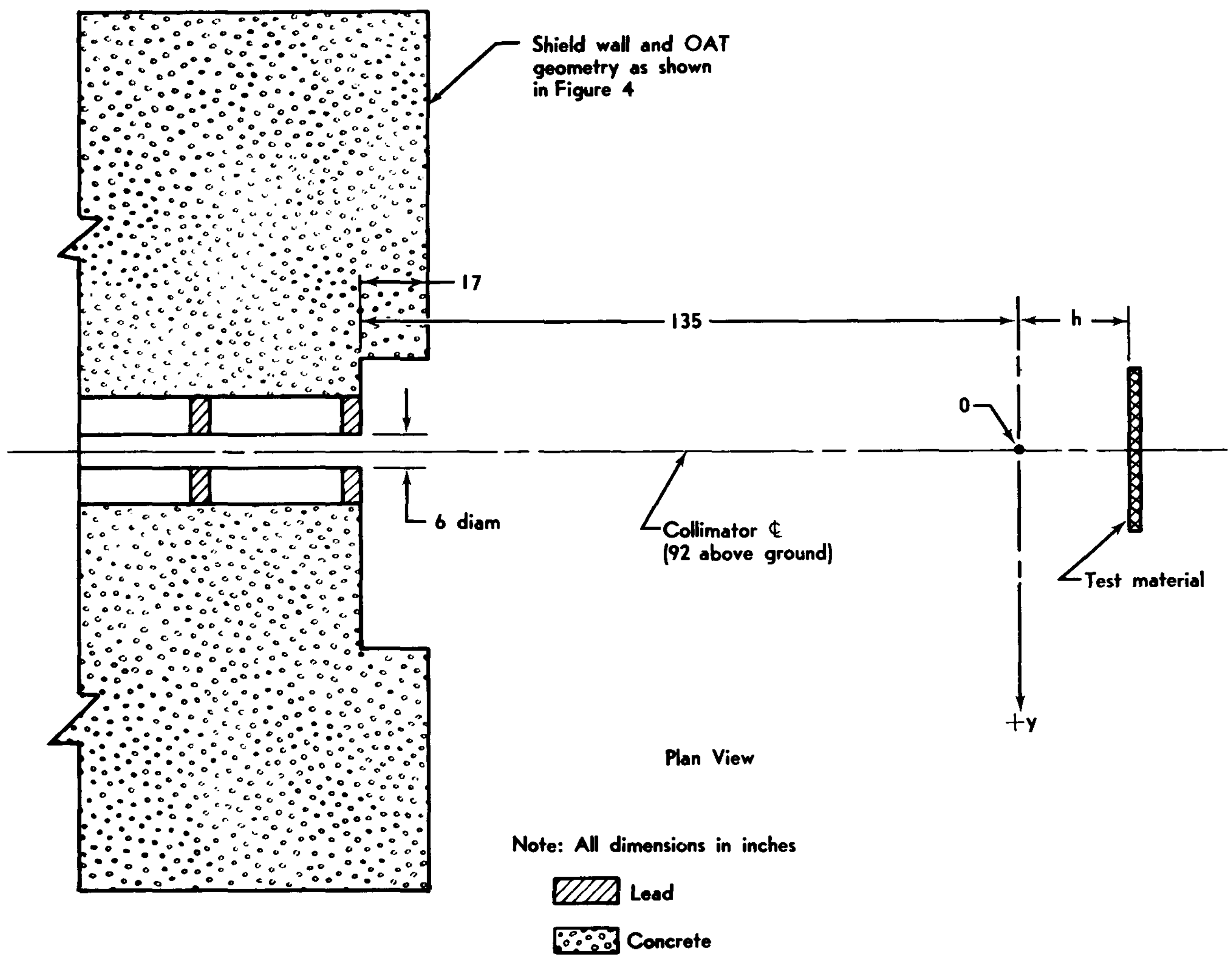


**Figure 8. OAT Geometry III**

# IV. EXPERIMENTAL PROCEDURES

A description of the various detector systems used during the experiment and, where necessary, a description of the data-reduction techniques are given in Sections 4.1.1 and 4.1.2.

During the early stages of the experiment, a concerted effort was directed toward determining the integrity of the experimental geometries used in the experiment. These procedures, as well as the results of the geometry checkouts, are described in Section 4.2.

## 4.1 Radiation Detection Methods

Required for the experiment were a variety of detectors to determine the fast-neutron and gamma-ray dose rates and energy spectra and the thermal- and fast-neutron fluxes.

### 4.1.1 Neutron Detectors

Fast-neutron dose rates were determined by means of the fast-neutron dosimeter (FND) described in Reference 3. The FND standardization was checked immediately prior to and following a particular series of measurements.

Bare and cadmium-covered enriched boron-trifluoride ($BF_3$) detectors (Ref. 4) were used to accumulate data on the neutron fluxes below and above the cadmium cutoff, which is approximately 0.5 ev. The $BF_3$ tubes were 0.565 inch in diameter and 8.5 inches long.

Subcadmium and fast-neutron fluxes were measured with various thermal and threshold foil detectors. Gold foils were used as thermal detectors. Fast-neutron flux data were obtained by using the $S^{32}(n,p)$, $Mg^{24}(n,p)$, $Al^{27}(n,p)$, and $Al^{27}(n,\alpha)$ reactions with their respective effective thresholds of 2.9, 6.3, 8.1, and 4.6 Mev. Following irradiation, the foil activities were determined by means of end-window counters coupled to automatic data processing equipment. The raw data were converted to neutron flux by the Foil Data IBM Reduction Code K-26.

Ilford L-2 nuclear-emulsion plates were used to determine the spectrum of fast neutrons transmitted through test materials of lead; Ilford K-1 plates were used in conjunction with 3% borated polyethylene test materials since these plates are less sensitive to gamma fogging when large thicknesses of polyethylene are used. A description of the plate-reading and data-reduction techniques are described in Reference 5.

4.1.2 Gamma-Ray Detectors

Gamma-ray dose rates were determined by means of the anthracene scintillation dosimeter (ASD) described in Reference 6.

A 3-crystal anticoincidence NaI(Tl) total-absorption gamma-ray spectrometer, designed at the GD/FW Nuclear Aerospace Research Facility and fabricated by the Harshaw Chemical Company, was used to investigate the production of secondary gamma rays within the test materials. Used in conjunction with the analyzer was an RCL 256-channel analyzer. A description of the spectrometer and the techniques used to analyze the pulse-height distributions accumulated using the spectrometer are described in Reference 7.

Spectral data on the penetration and scattering of primary gamma rays were obtained with a 5-in.-diam by 4-in.-long single crystal NaI(Tl) gamma-ray spectrometer coupled to the RCL 256-channel analyzer. The pulse-height distributions, corrected for background, were converted to energy spectra by a IBM-7090 program and a 36 x 36 inverse response matrix which was formulated from the Q-32 code.

## 4.2 Experimental Geometry Checkout

To establish the integrity of the experimental geometry, a series of radiation measurements was made which were designed to determine (1) the importance of neutron streaming, leakage, and air scattering relative to the direct-beam radiation; (2) the extent to which the test material approximated an infinite-slab geometry; and (3) the degree of symmetry of the direct beam of radiation from the ASTR.

The magnitude and distribution of neutron streaming was determined by flooding the source collimator with water and then obtaining the fast-neutron dose rate and subcadmium and epicadmium $BF_3$ count rate as a function of $\Theta$ for $\Theta \leq \pm 60°$. It was established that the streaming of fast neutrons contributed little to the regular experimental data, whereas streaming of subcadmium neutrons contributed as much as 80% to the experimental values at large angles and thicknesses of borated polyethylene test materials. Regardless of the magnitude of the streaming - which had an angular distribution independent of the test-material configuration - all experimental data were corrected for the effect of streaming.

Shown in Figure 9 are the fast-neutron dose-rate distributions on the exit side of the borated polyethylene as a function of $y$. These data show that beam symmetry is good. The data also provide information on the extent to which an infinite slab geometry is approximated. As an example, consider the fast-neutron dose rate, $D_n(y)$, as a function of $y$ for a 9-in.-thick borated polyethylene slab. Performing the integration

$$\int_{y=0}^{y} D_n(y)\ 2\pi y\ dy$$

shows that integrating to $y = 30$ inches and $y = 50$ inches gives results little different one from the other, $y = 50$ inches being the maximum value of $y$ mapped. Remembering that the half width of the polyethylene slabs is 24 inches and assuming 50 inches to be the limiting value of $y$, the integral ratio $R_n$ is calculated:

$$R_n = \left[\int_{y=0}^{y} D_n(y)\ 2\pi y\ dy\right]\left[\int_{y=0}^{50''} D_n(y)\ 2\pi y\ dy\right]^{-1} .$$

This ratio is an expression with which to evaluate the degree to which the slab approximates an infinite-slab condition for the transmission of neutrons. $R_n$, as a function of $y$, for a 9-in.-thick borated polyethylene slab is shown in Figure 10 where it is

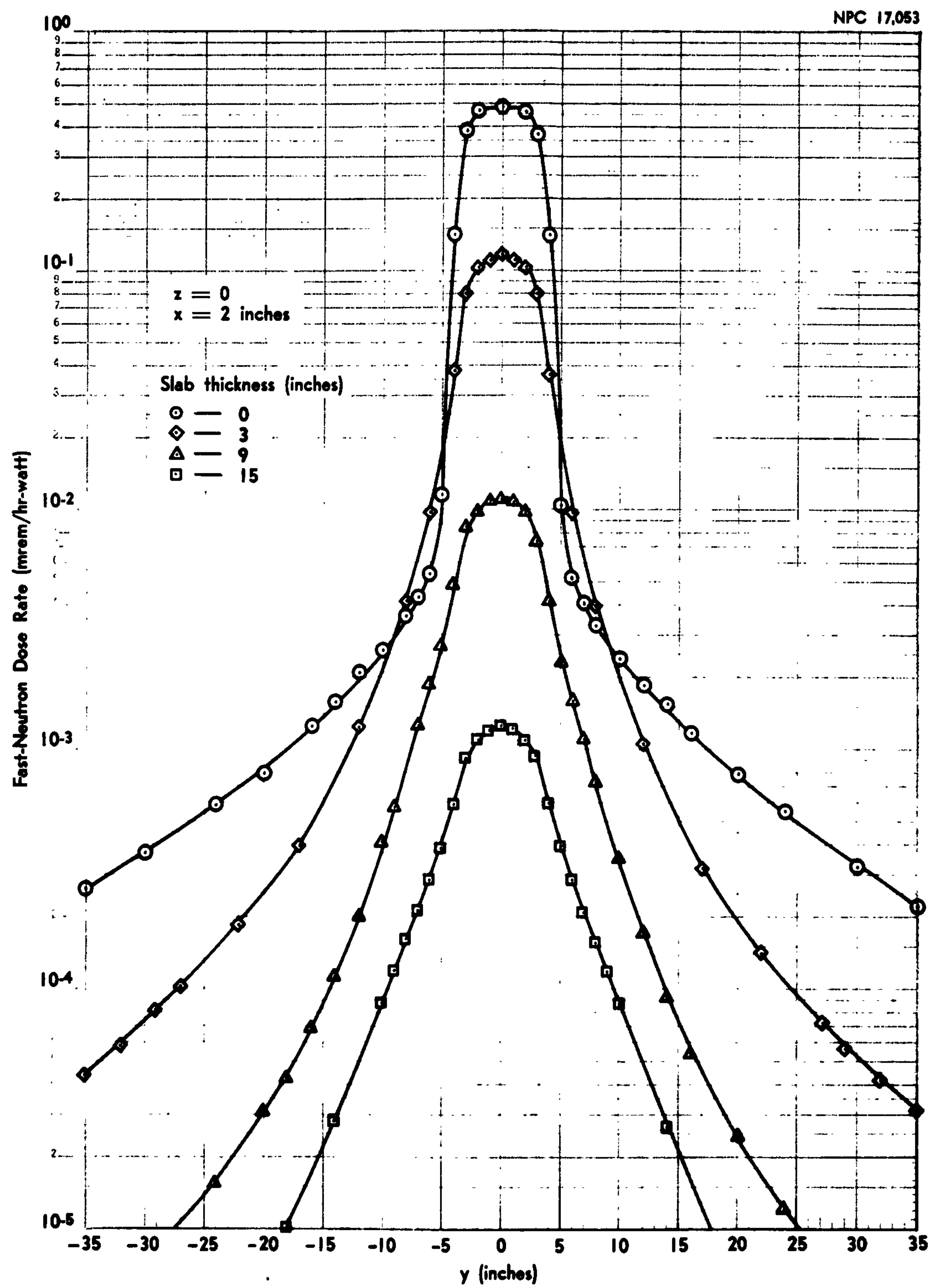


**Figure 9. Fast-Neutron Dose-Rate Map across Exit Face of Particular Thicknesses of 3% Borated Polyethylene Slabs**

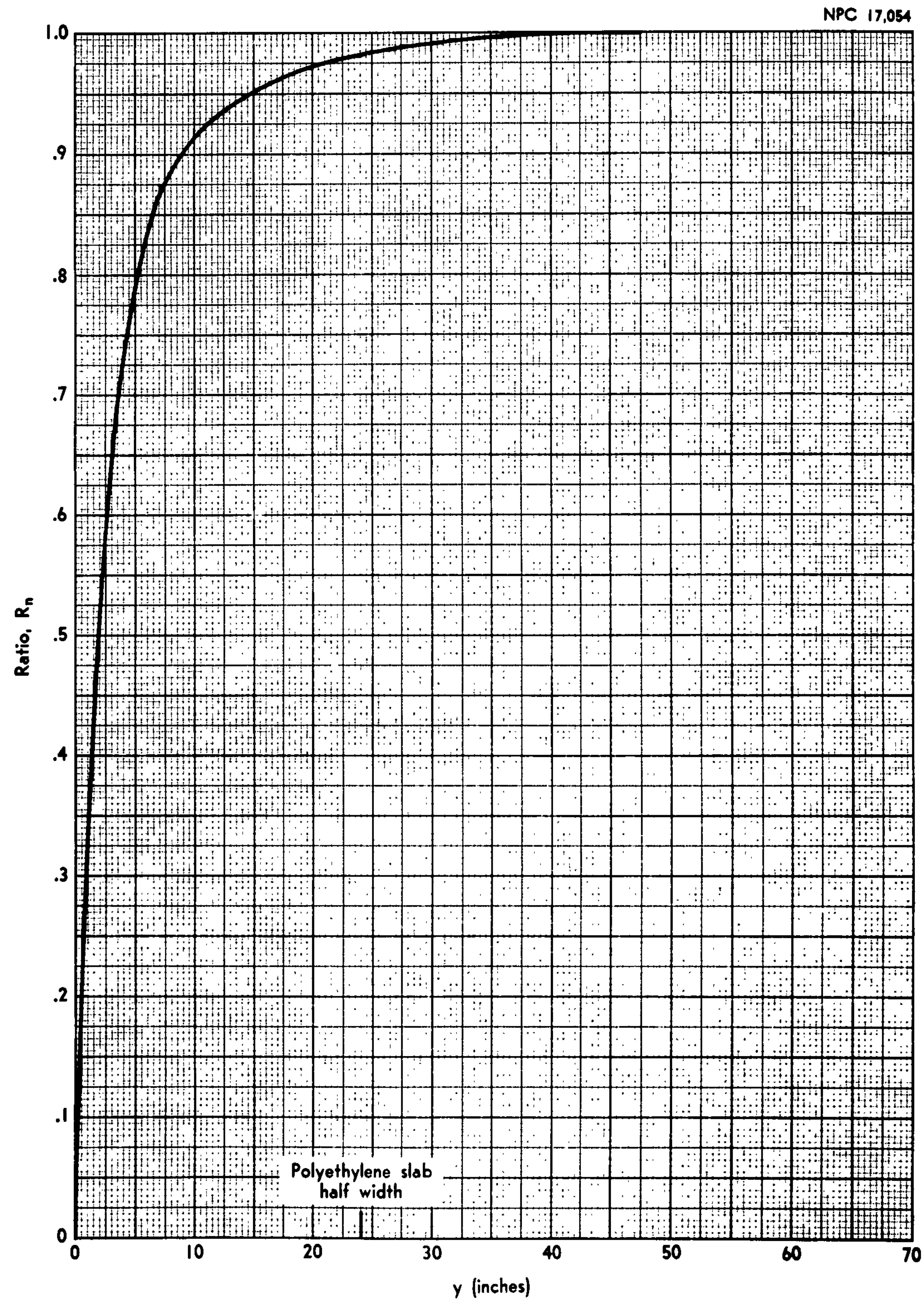


**Figure 10. Infinite-Slab Approximation for 9-Inch-Thick Slab of 3% Borated Polyethylene**

evident that the slab rapidly approaches the infinite-slab condition with increasing values of y. At y = 24 inches, $R_n$ is equal to 0.98, which signifies that 98% of the emergent fast-neutron dose rate is transmitted through the slab within the slab boundary; thus, the slab closely approximates an infinite-slab condition.

Insofar as geometrical effects are concerned, a comparison of bare and collimated fast-neutron dose-rate data obtained at various values of the angle θ provided a measure of the accuracy of the experiment. Because the difference between the bare and collimated data was small, it was concluded, in conjunction with previously described measurements, that the experimental measurements could be used for comparison with angular distribution calculations for infinite plane sources.

## V. RESULTS AND DISCUSSION

The experimental results reported below include all data accumulated except the angular distribution of the number-energy flux for fast neutrons and gamma rays. For the sake of clarity, subcadmium and epicadmium fluxes will be referred to as thermal and epithermal fluxes, respectively.

### 5.1 OAT Geometry I

Data presented for the experimental geometry shown in Figure 4, the high neutron-to-gamma ratio configuration, include the fast-neutron source term, the angular distribution of fast-neutron dose rate, the relative thermal- and epithermal-neutron flux, the neutron flux distributions at particular depths along the centerline of the test materials, and the angular distribution of secondary gamma rays produced within and emerging uncollided from the test materials.

#### 5.1.1 Source Term of Fast Neutrons

The spectrum of fast neutrons and the flux of thermal neutrons incident to the test materials are shown in Figure 11. Integration of the spectrum over energy shows that the fast-neutron to thermal-neutron flux ratio is approximately 8.

#### 5.1.2 Angular Distribution of Neutron Dose Rate and Flux

The fast-neutron dose rate angular map of the source-collimator at a slab-detector separation distance of 192 inches and for no test material in position is shown in Figure 12.

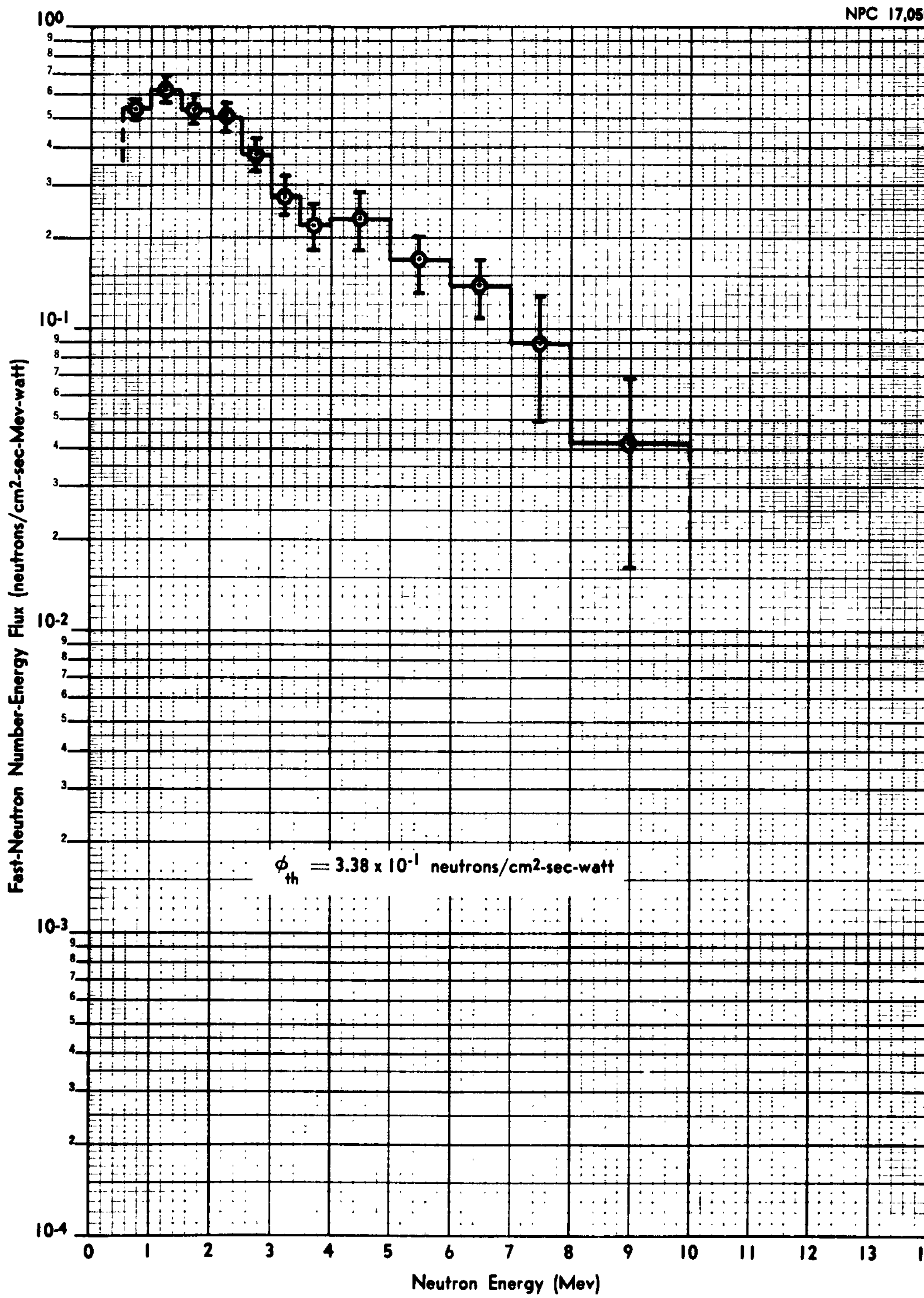


**Figure 11. Spectrum of Fast Neutrons Incident to Test Materials ($\theta$, x, y, z = 0)**

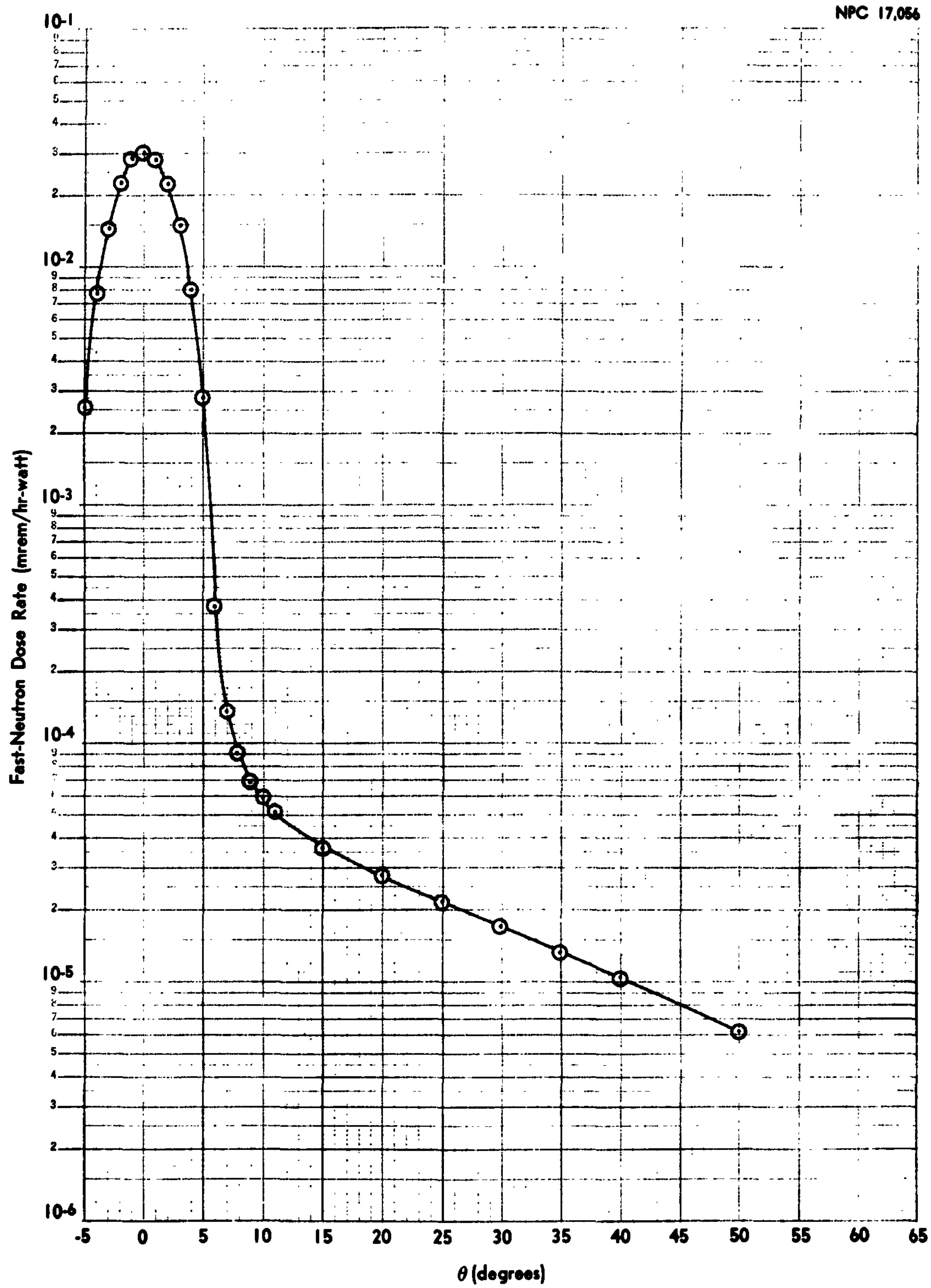


**Figure 12. Angular Distribution of Fast-Neutron Dose Rate: Collimator Map for No Test Material in Position (R = 192 Inches)**

Shown in Figure 13 are the angular distributions of fast-neutron dose rate for borated polyethylene slab thicknesses of 3, 6, 9, 12, and 15 inches. These distributions show the distinct separation of direct-beam and scattered components of radiation transmitted from the test material. Also obvious is the fact that the rate of change in dose rate as a function of the angle $\theta$ in the scattered portion of the distribution is essentially independent of material thickness for the thicknesses investigated.

The angular distributions of fast-neutron dose rate for lead thicknesses of 2, 4, and 6 inches are shown in Figure 14. It appears that equilibrium of the scattered component of fast-neutron dose rate is rapidly approached in going from a lead thickness of 2 inches to one of 4 inches.

The angular distributions of relative thermal- and epithermal-neutron flux obtained from bare and cadmium-covered $BF_3$ detectors for particular thicknesses of borated polyethylene are shown in Figures 15 and 16. The rapid disappearance of the direct-beam component of thermal-neutron flux is evidenced in Figure 15 by the shape of the distributions and by the fact that meaningful data were obtained for a maximum material thickness of only 6 inches. An examination of the epithermal-neutron flux distributions (Fig. 16) for borated polyethylene again reflect the fact that equilibrium is rapidly reached with increasing thickness of the hydrogenous material.

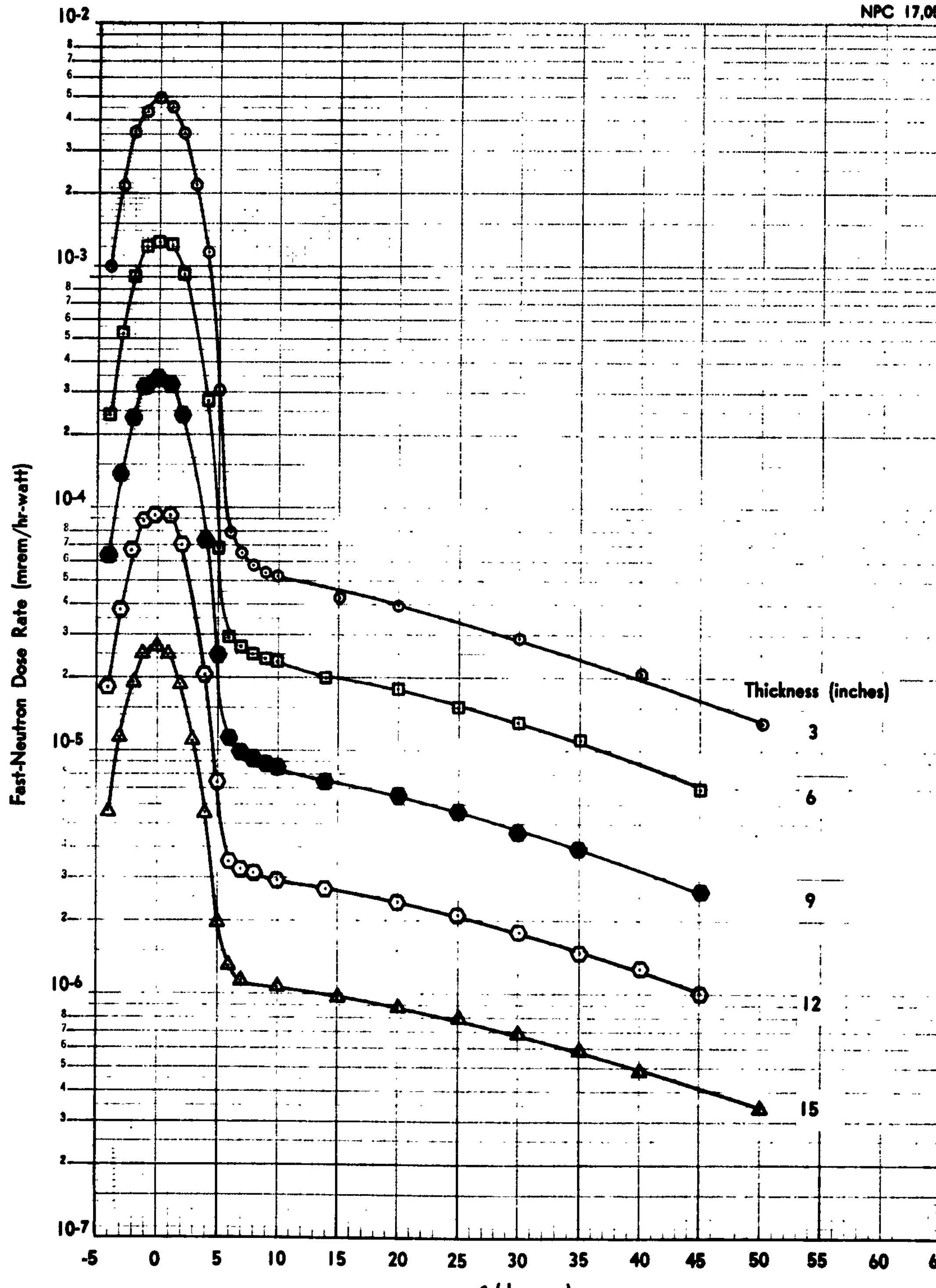


**Figure 13. Angular Distribution of Fast-Neutron Dose Rate from Particular Thicknesses of 3% Borated Polyethylene Slabs (R = 192 inches)**

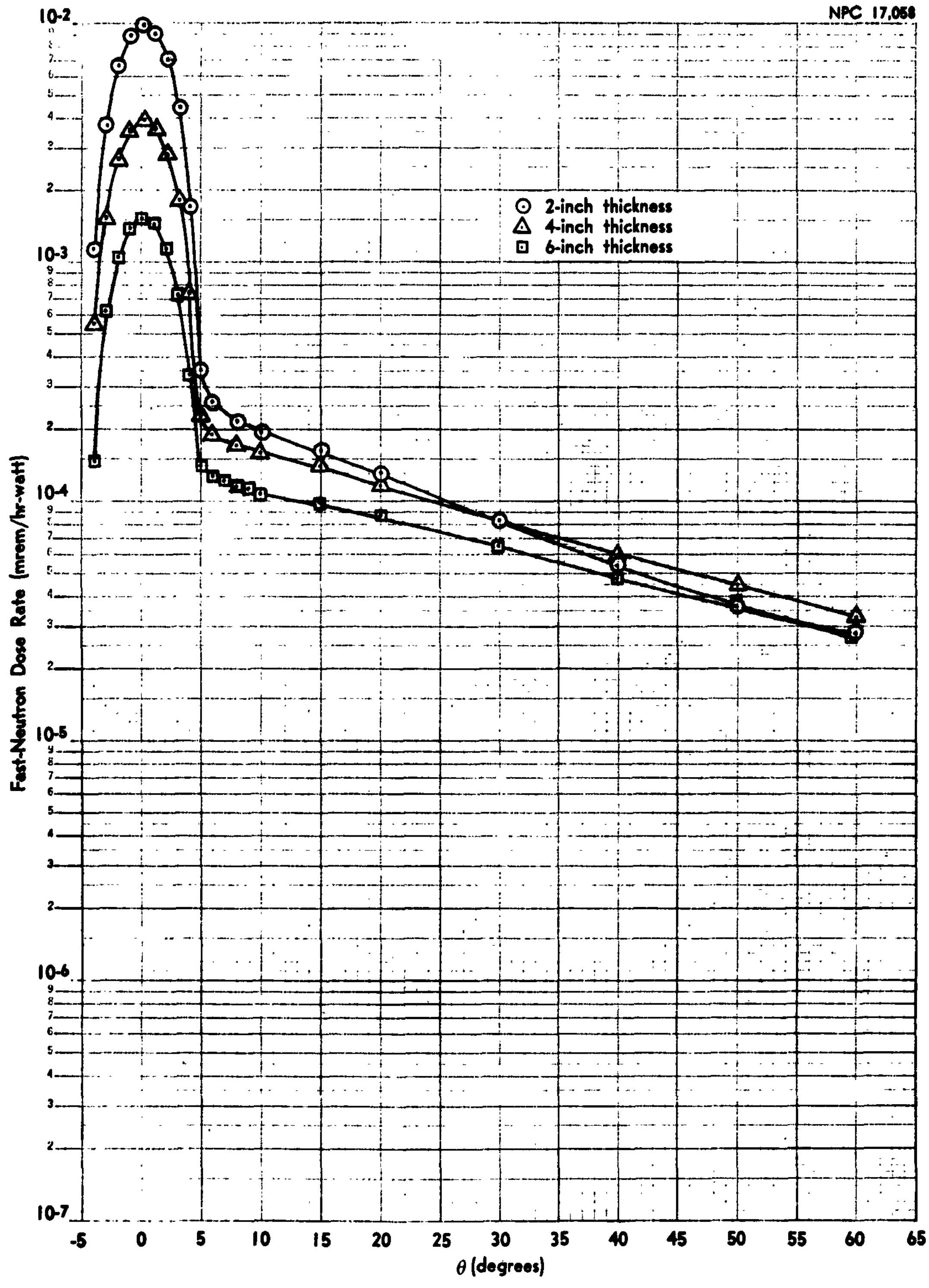


**Figure 14. Angular Distribution of Fast-Neutron Dose Rate from Particular Thicknesses of Lead Slabs (R = 192 Inches)**

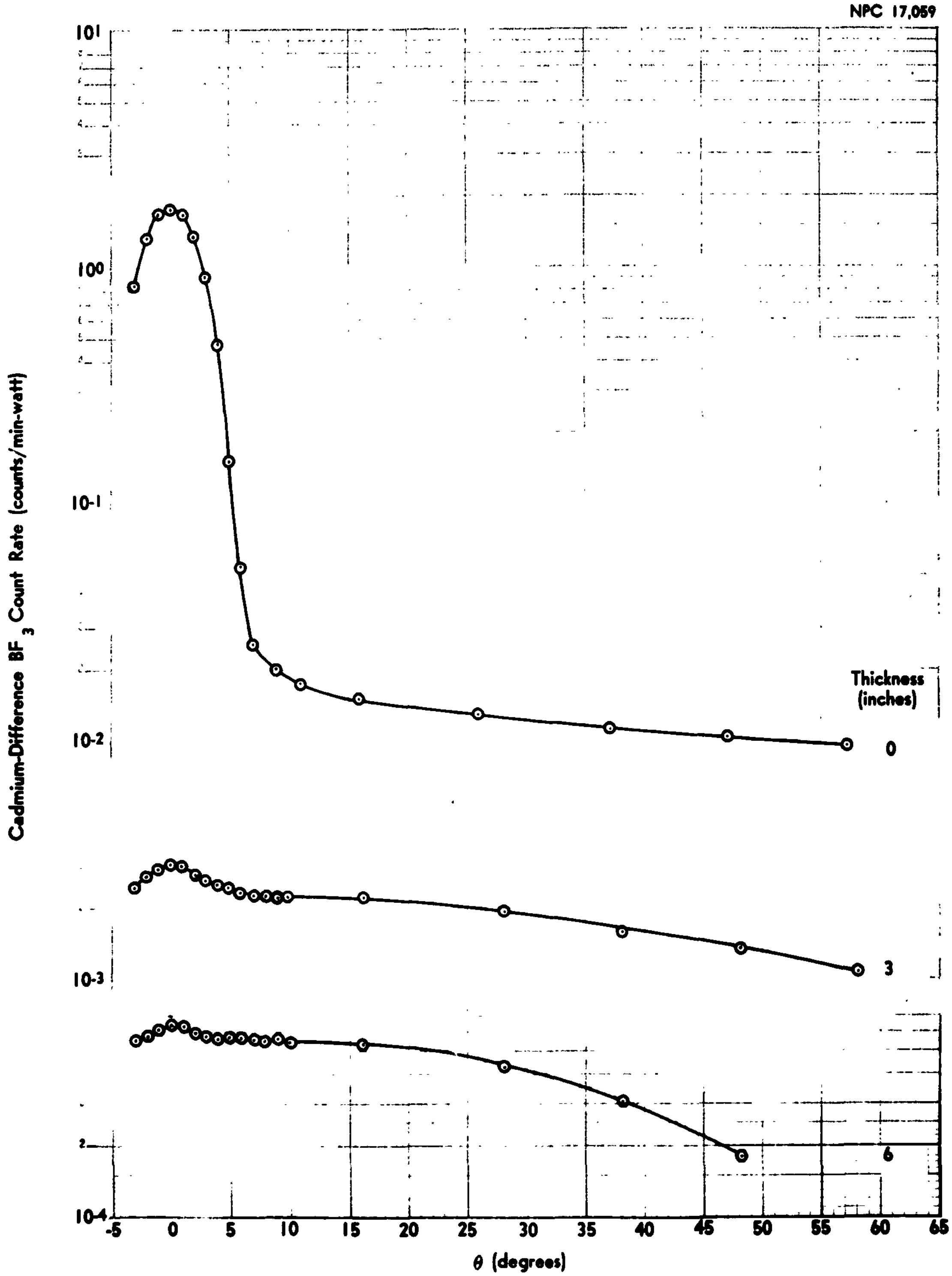


**Figure 15. Angular Distribution of Relative Thermal-Neutron Flux from Various Thicknesses of 3% Borated Polyethylene Slabs (R = 192 Inches)**

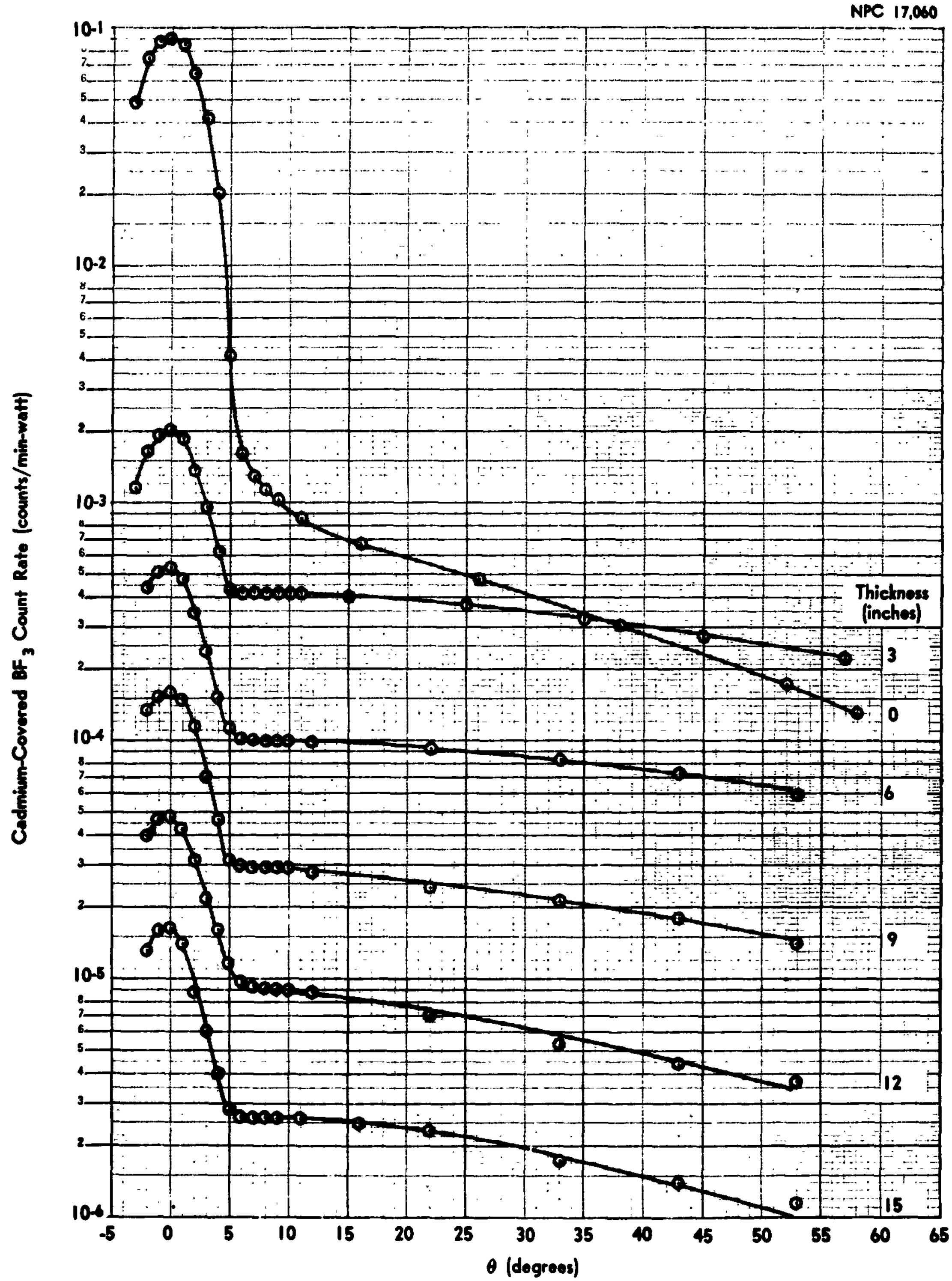


**Figure 16. Angular Distribution of Relative Epithermal-Neutron Flux from Various Thicknesses of 3% Borated Polyethylene Slabs (R = 192 inches)**

The angular distributions of the thermal- and epithermal-neutron flux for various thicknesses of lead are shown in Figures 17 and 18. These distributions reflect the low neutron absorption properties of lead, particularly for thermal neutrons, in that the shape and magnitude change little with increasing thickness for angles greater than approximately 10 degrees.

### 5.1.3 Neutron Flux Distributions Within Test Materials

The use of threshold foil detectors to measure neutron flux requires that an effective threshold energy be assigned for the various reactions involved. The effective thresholds used are those previously described and shown in Figures 19 through 24.

The distribution of neutron flux along the centerline of 3-, 6-, and 9-in.-thick slabs of borated polyethylene is shown in Figures 19, 20, and 21, respectively. Shown in Figures 22, 23, and 24, respectively, are the neutron flux distributions along the centerline of 2-, 4-, and 6-in.-thick slabs of lead.

For thermal neutrons, the effect of the finite slab boundary is noticeable for both materials investigated. A comparison of the lead and polyethylene data shows that the attenuation properties of the two materials are essentially the same for neutrons above 6.3 Mev in energy.

### 5.1.4 Secondary Gamma-Ray Production

Data-reduction procedures used to evolve the gamma-ray flux distributions described below include corrections for detector

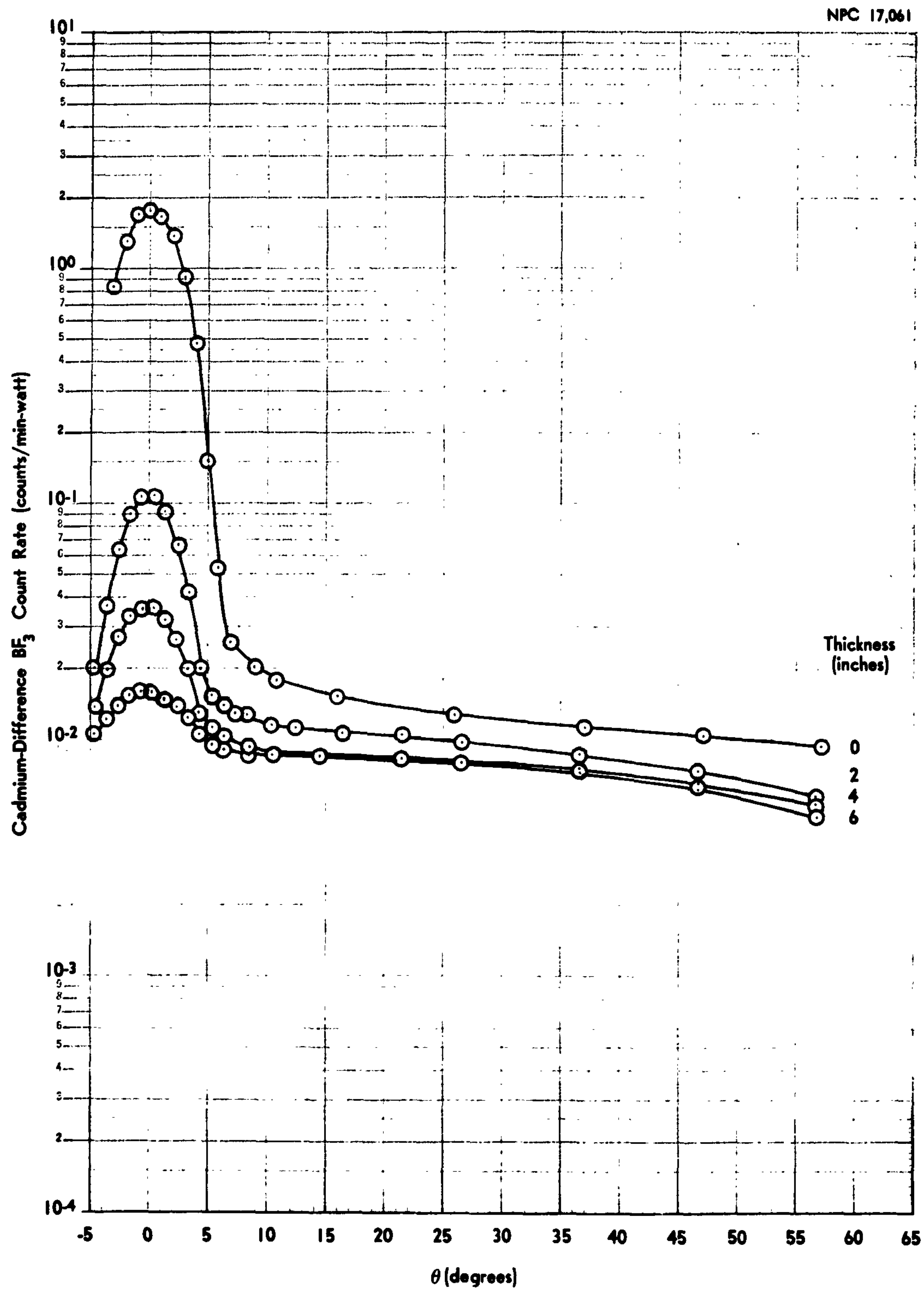


**Figure 17. Angular Distribution of Relative Thermal-Neutron Flux from Various Thicknesses of Lead Slabs (R = 192 Inches)**

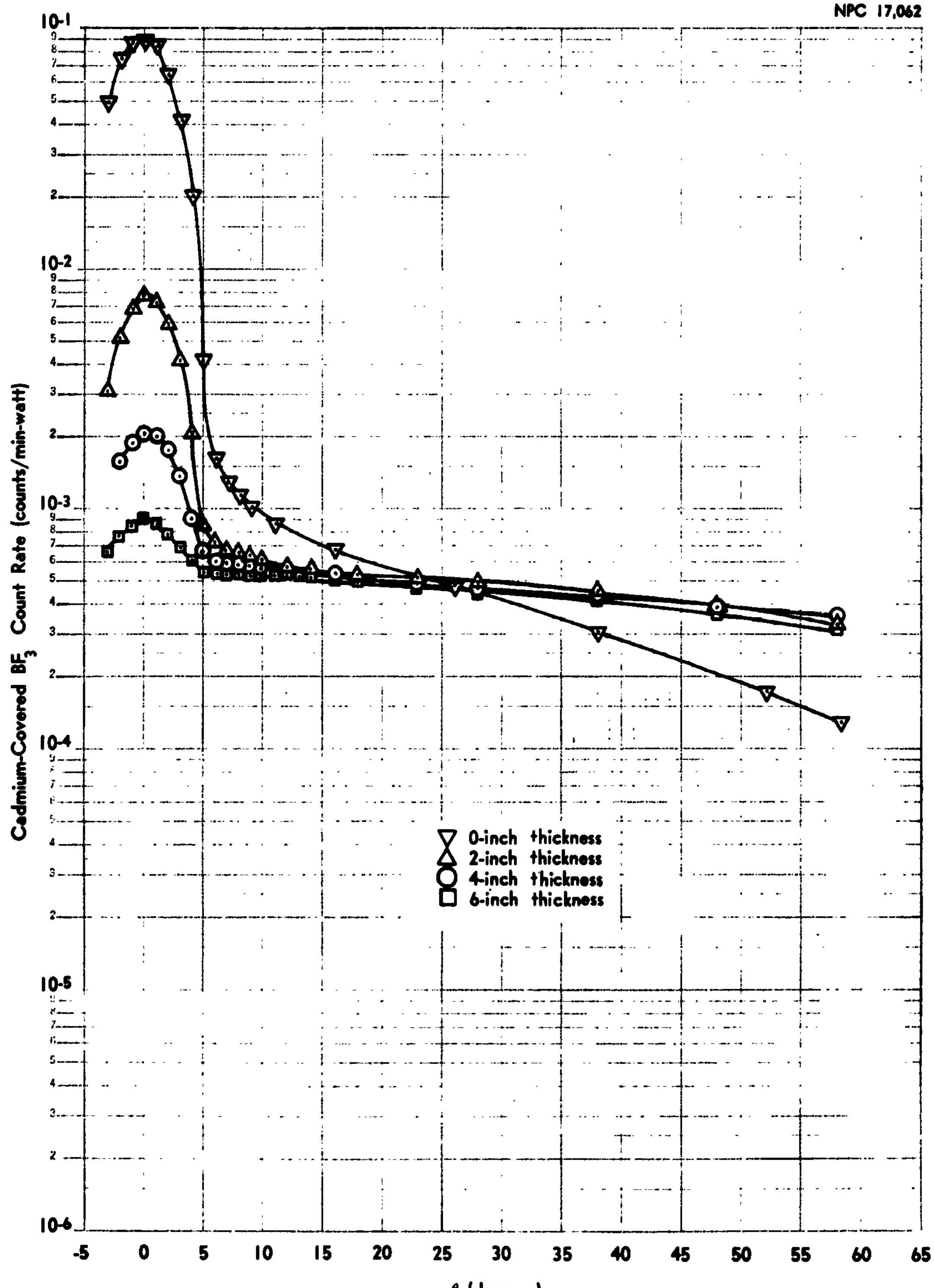


Figure 18. Angular Distribution of Relative Epithermal-Neutron Flux from Various Thicknesses of Lead Slabs (R = 192 Inches)

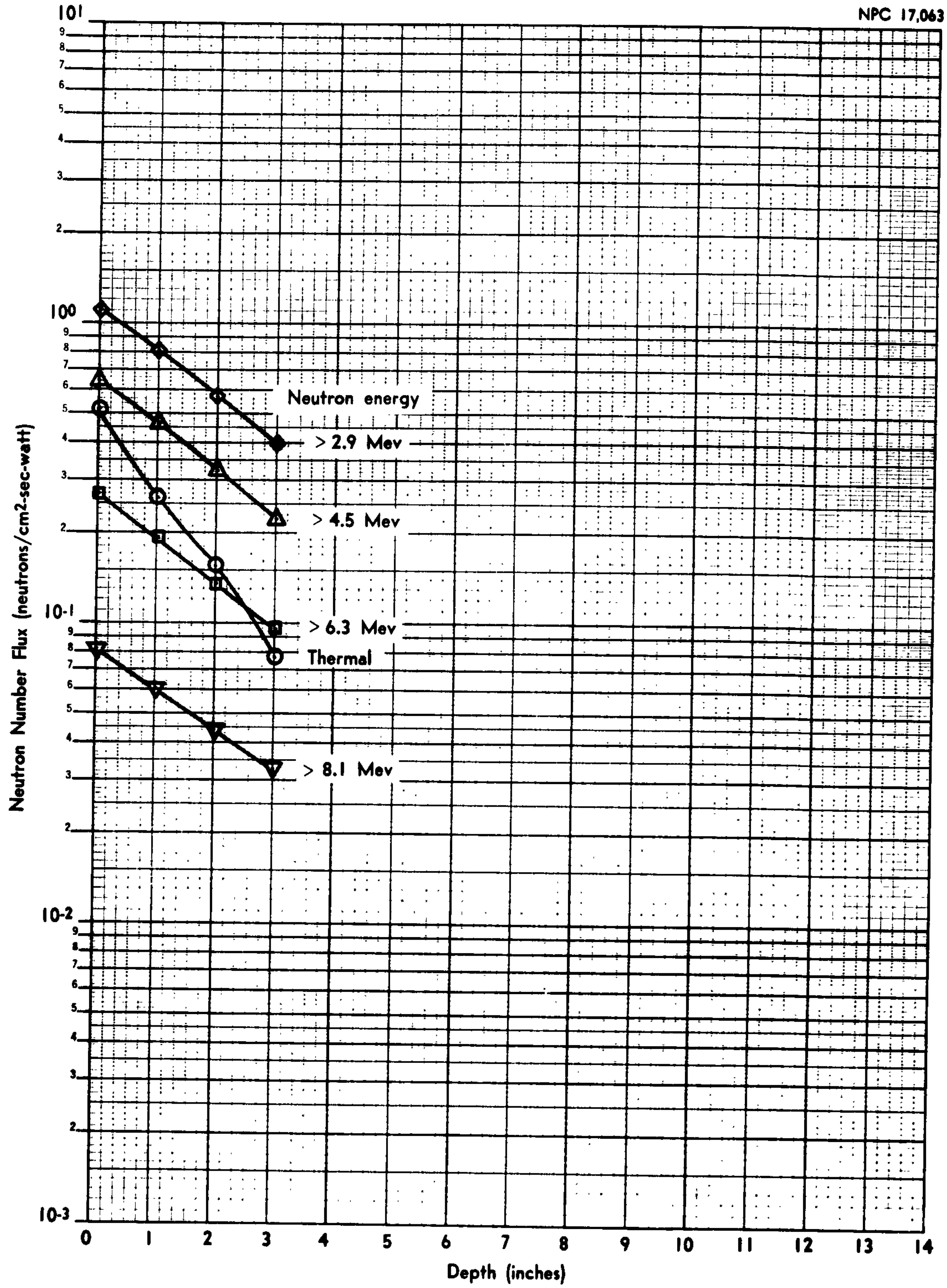


**Figure 19. Distribution of Neutron Flux along Centerline of a 3-Inch-Thick Slab of 3% Borated Polyethylene**

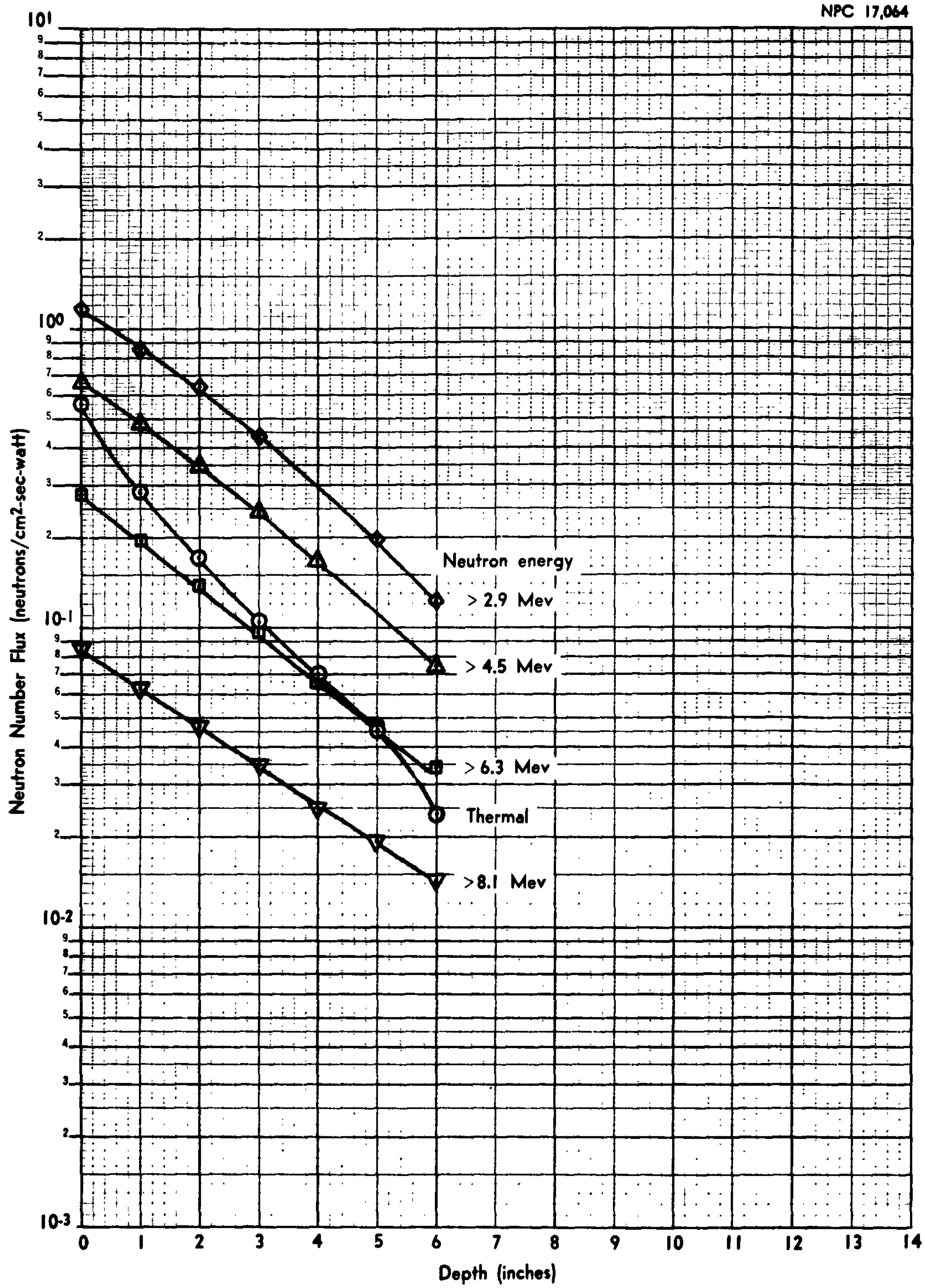


**Figure 20. Distribution of Neutron Flux along Centerline of a 6-Inch-Thick Slab of 3% Borated Polyethylene**

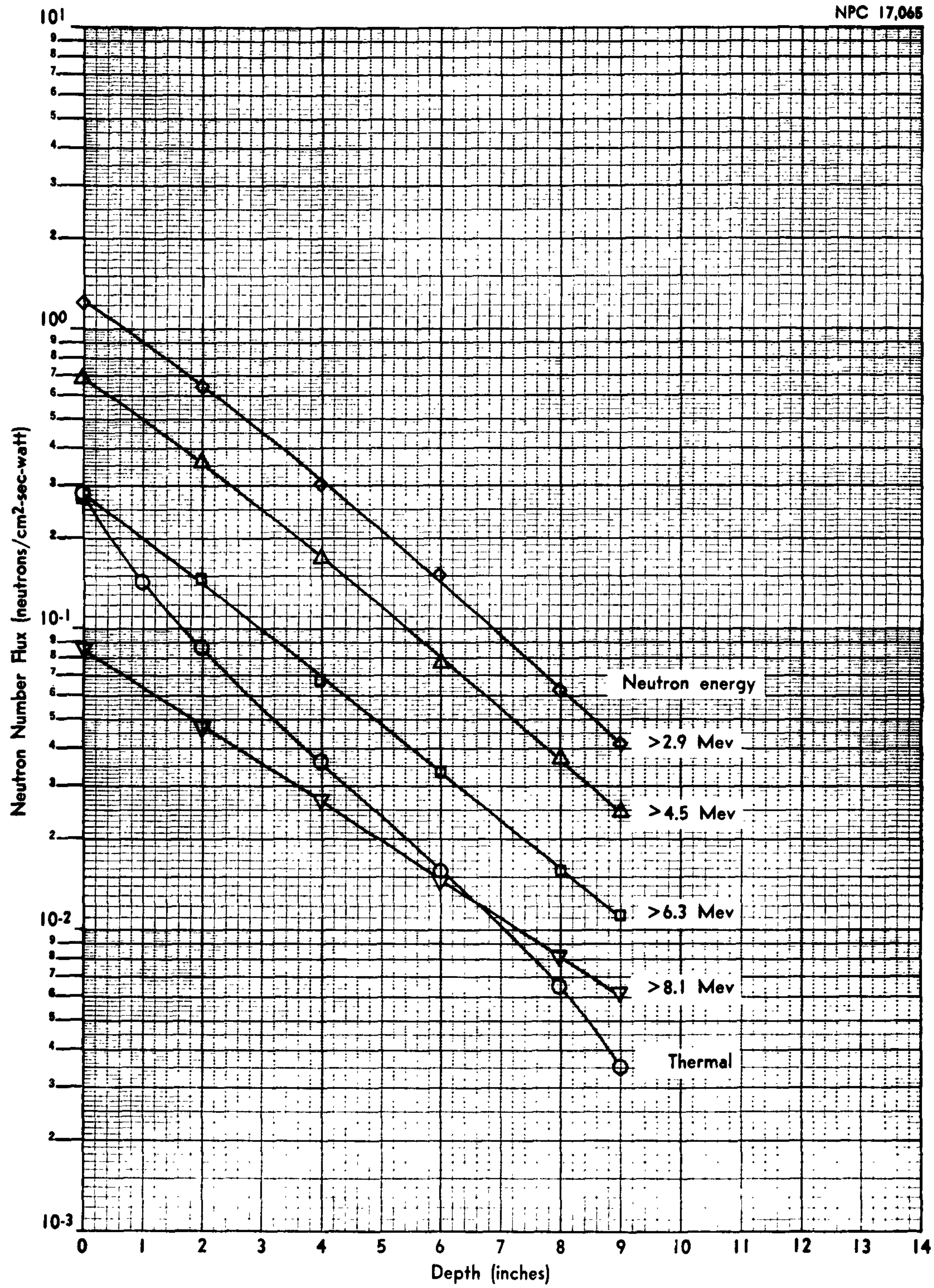


**Figure 21. Distribution of Neutron Flux along Centerline of a 9-Inch-Thick Slab of 3% Borated Polyethylene**

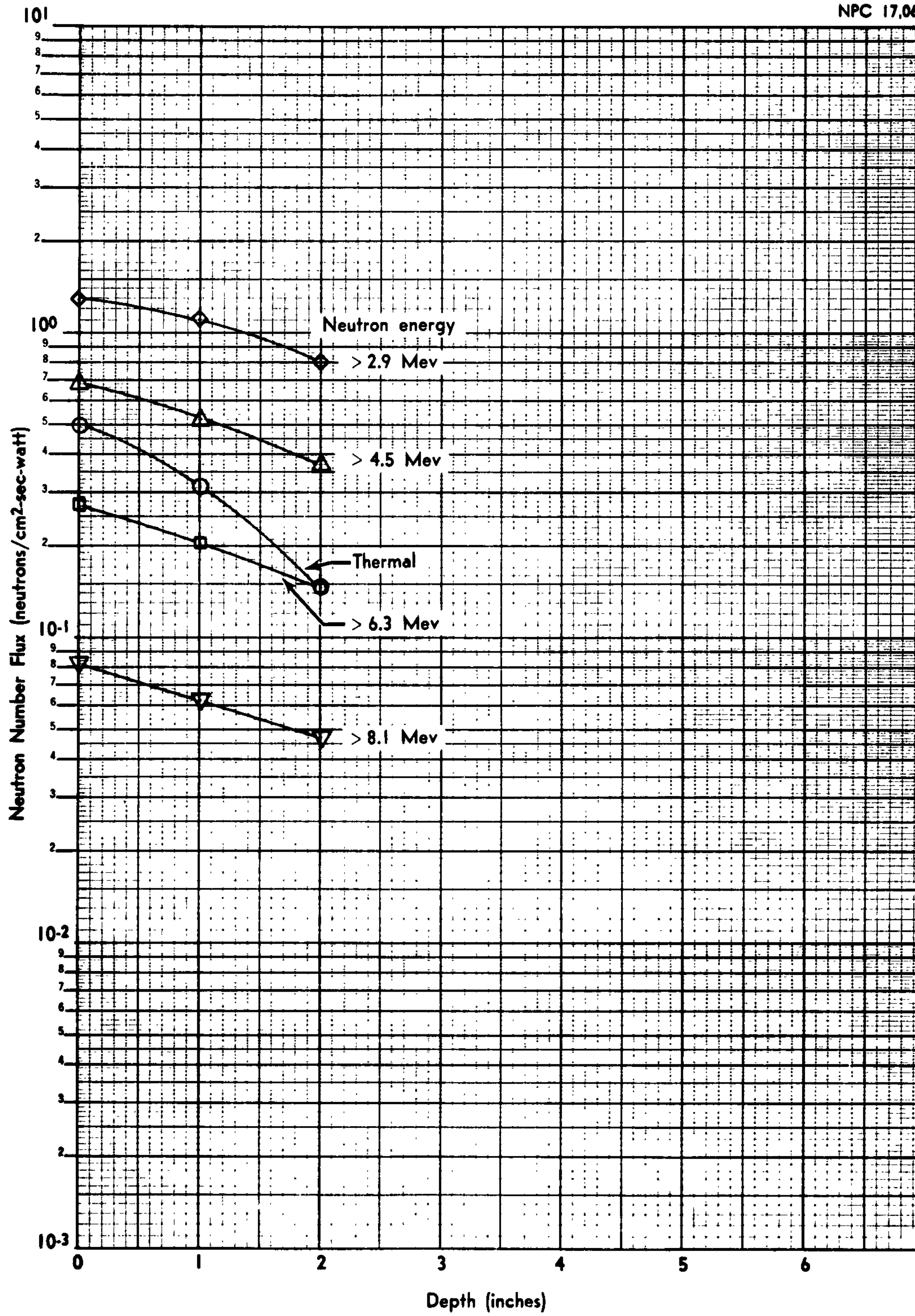


**Figure 22. Distribution of Neutron Flux along Centerline of a 2-Inch-Thick Slab of Lead**

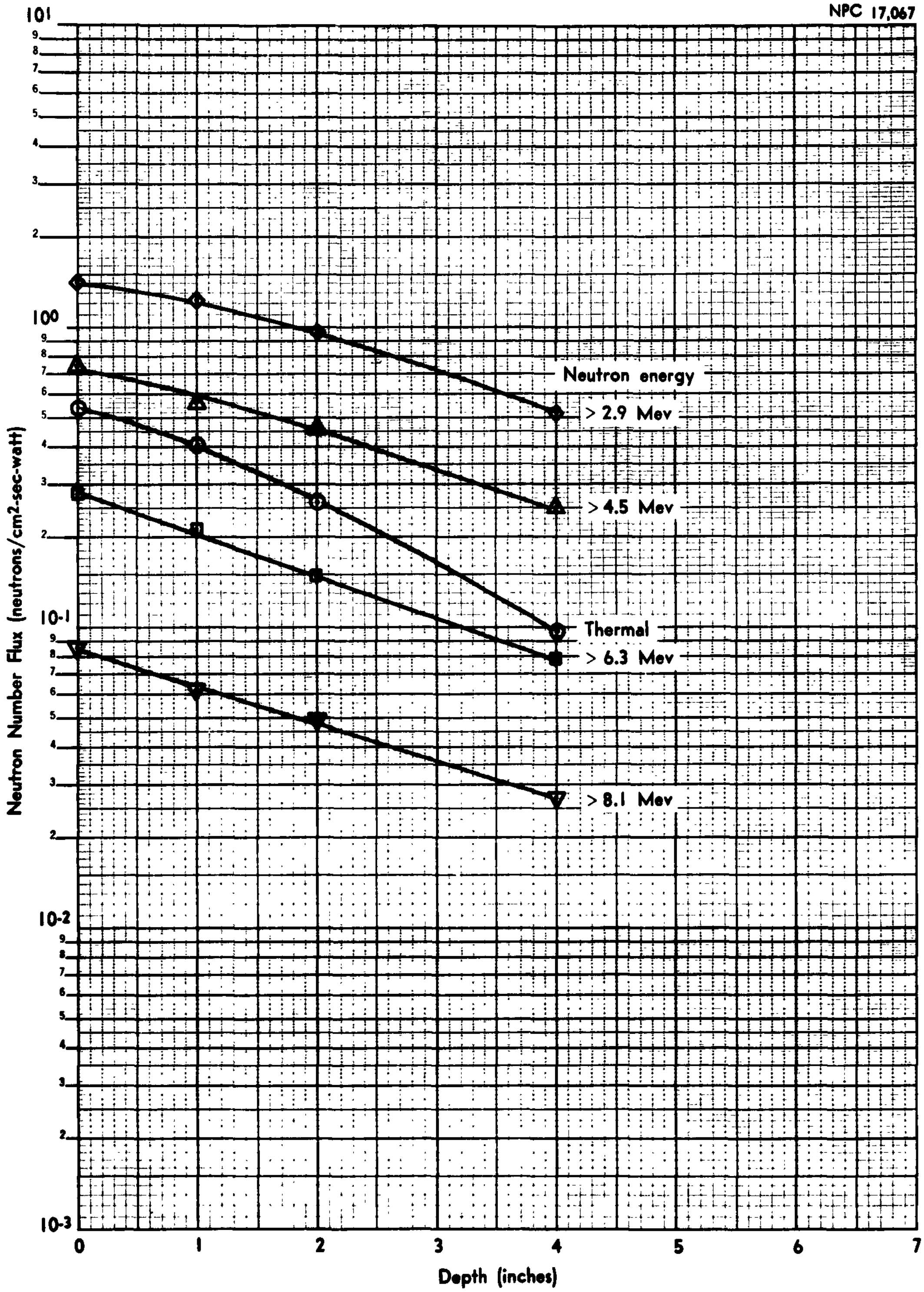


**Figure 23. Distribution of Neutron Flux along Centerline of a 4-Inch-Thick Slab of Lead**

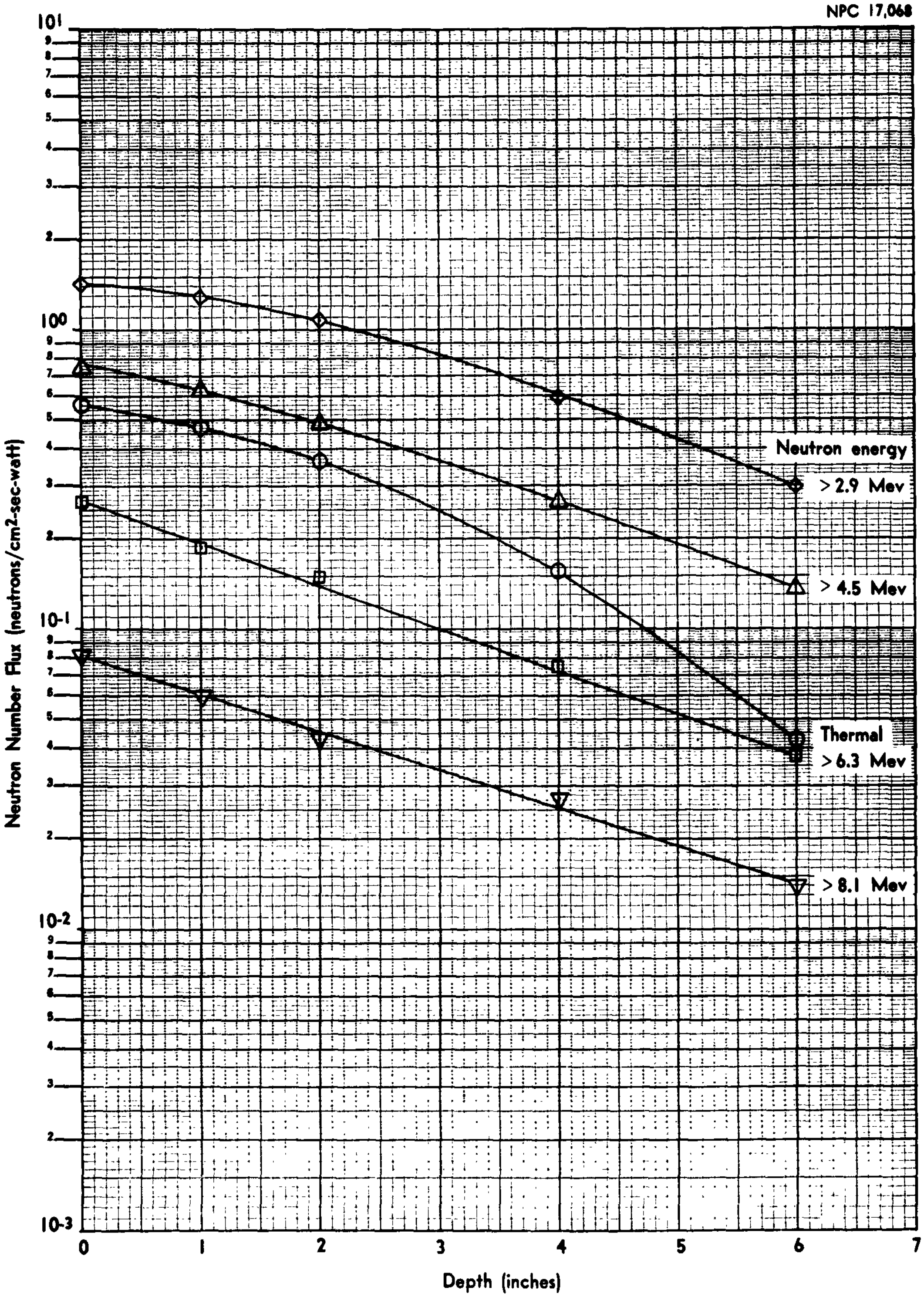


**Figure 24. Distribution of Neutron Flux along Centerline of a 6-Inch-Thick Slab of Lead**

collimator edge penetration by the gamma rays of interest; the data-reduction techniques are fully described in Appendix B of Reference 7.

Representative pulse-height distributions showing structure attributed to secondary gamma rays from borated polyethylene and lead are shown in Figures 25 and 26. Figure 25 shows the pulse-height distribution accumulated at an angle of $\theta = 60^{\circ}$, the test material being a 6-in.-thick slab of 3% borated polyethylene. Identified in the distribution are total absorption peaks attributed to 2.23- and 4.45-Mev gamma rays produced in $H(n_{th},\gamma)$ and $C^{12}(n,n'\gamma)$ reactions, respectively.

The pulse-height distribution shown in Figure 26 was obtained at an angle of $\theta = 45^{\circ}$ with a 2-in.-thick slab of lead as the test material. The total absorption peak at channel number 67.5 is attributed to 2.615-Mev gamma rays produced in the $Pb^{208}(n,n'\gamma)$ reaction.

The angular distributions of 2.23-Mev gamma rays emerging from particular thicknesses of borated polyethylene, following the $H(n_{th},\gamma)$ reaction, are shown in Figure 27. The dotted curve, being qualitative, was evolved by cross-plotting the experimental data and extrapolating to $\theta = 0^{\circ}$. Data were not obtained for $\theta < 15^{\circ}$ because of the large contribution of scattered primary gamma rays.

Shown in Figure 28 are the angular distributions of 4.45-Mev gamma rays emerging from various thicknesses of borated polyethylene slabs following $C^{12}(n,n'\gamma)$ reactions within the material. The

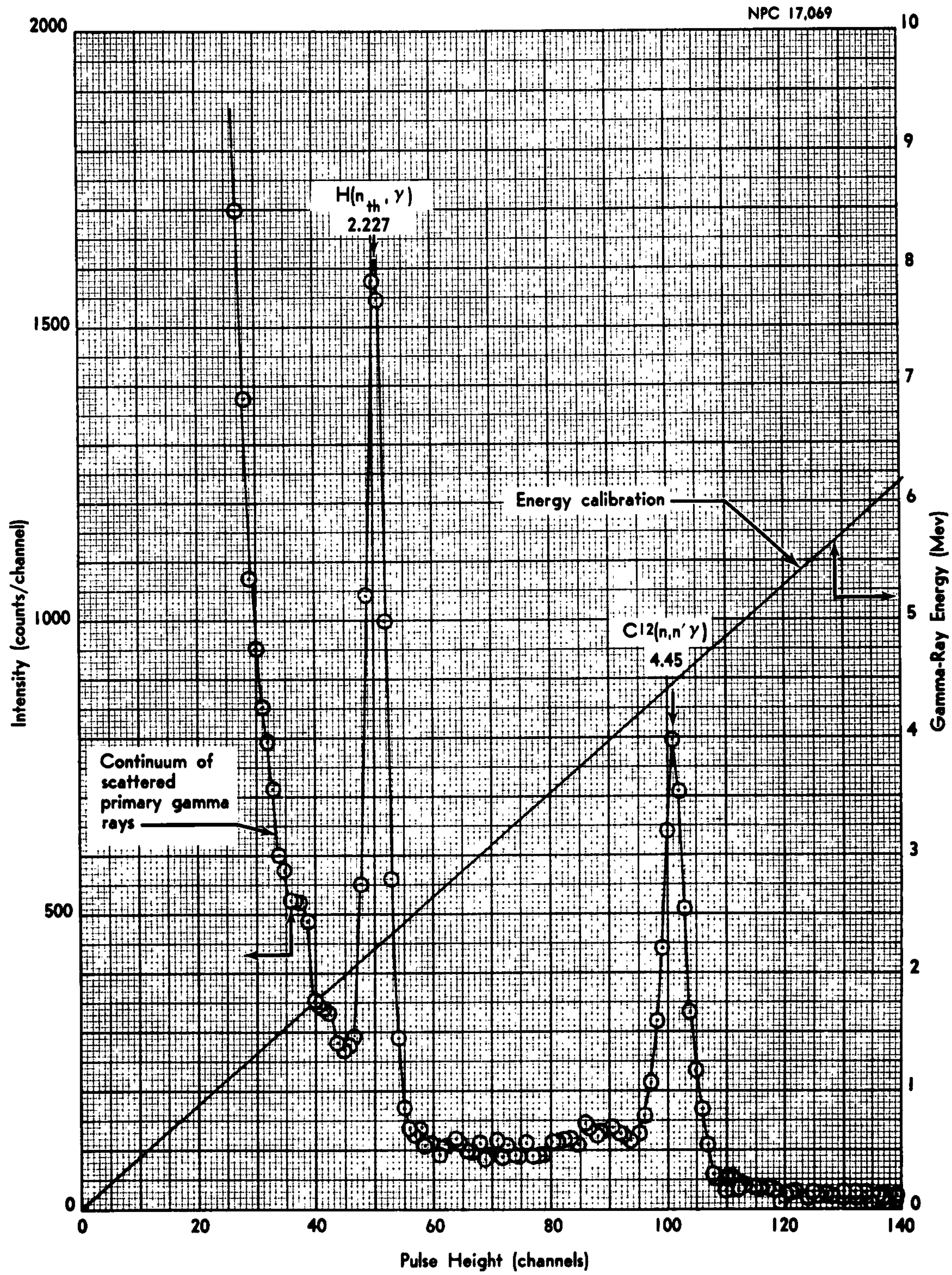


**Figure 25. Pulse-Height Spectrum of Secondary Gamma Rays from a 6-Inch-Thick Slab of 3% Borated Polyethylene ($\theta = 60°$, R = 188 Inches)**

THIS

PAGE

IS

MISSING

IN

ORIGINAL

DOCUMENT

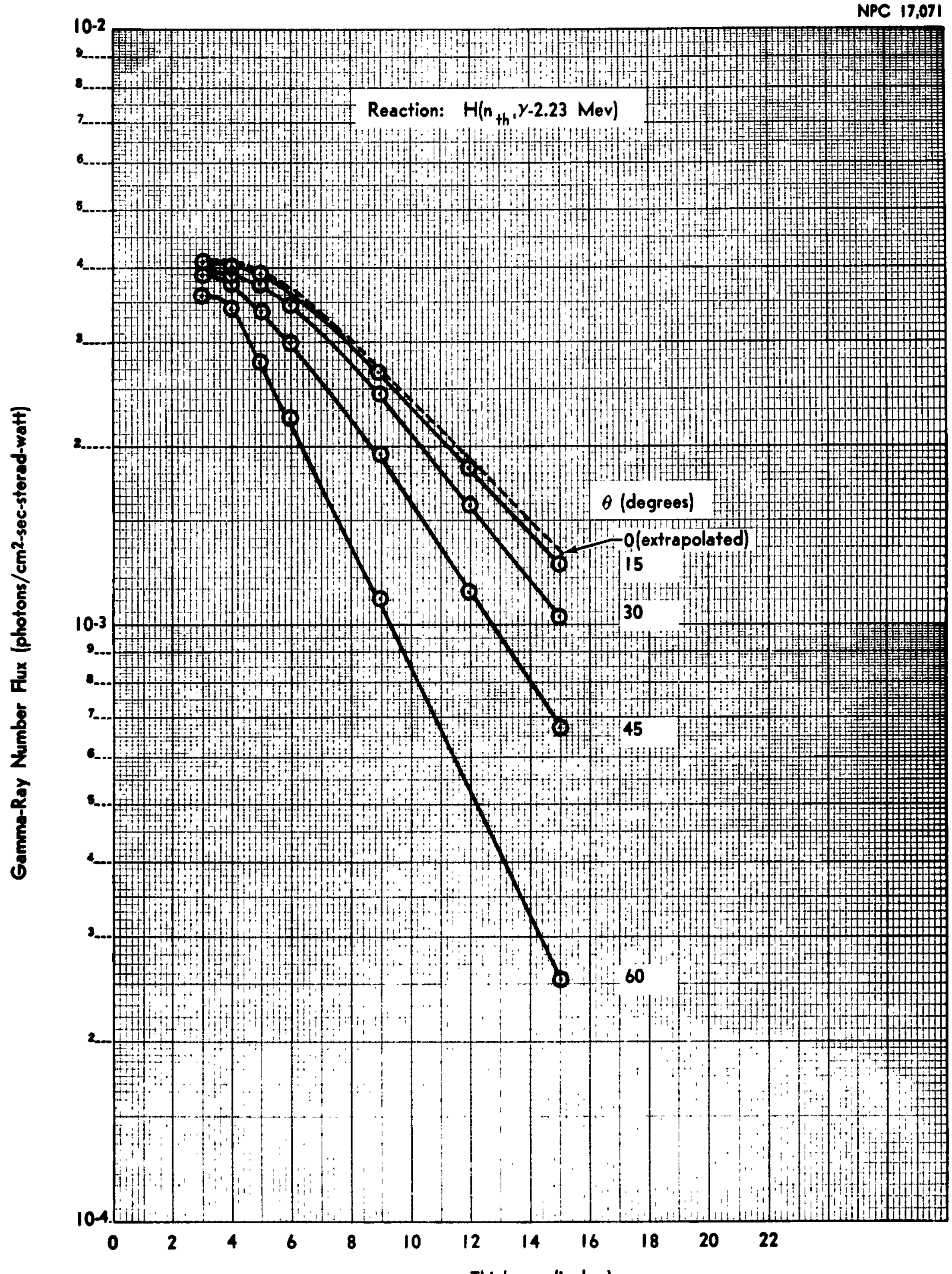


**Figure 27. Angular Distribution of Capture-Produced Secondary Gamma Rays from Particular Thicknesses of 3% Borated Linear Polyethylene Slabs (R = 188 Inches)**

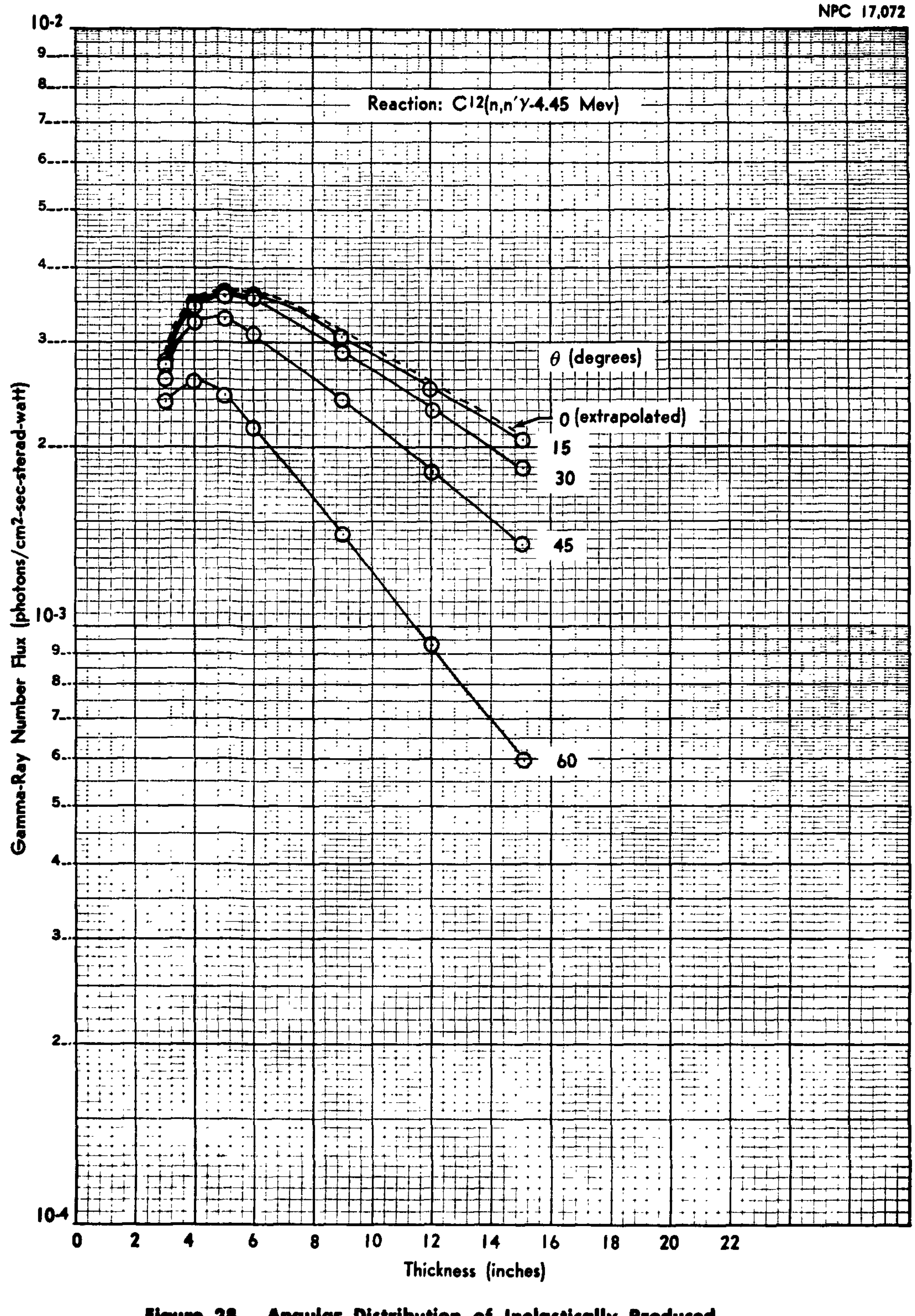


**Figure 28. Angular Distribution of Inelastically Produced Secondary Gamma Rays from Particular Thicknesses of 3% Borated Linear Polyethylene Slabs (R = 188 Inches)**

dotted curve was determined in the same manner as that described for Figure 27.

The data shown in Figure 29 are the angular distributions of 2.615-Mev gamma rays [$Pb^{208}(n,n'\gamma)$ reaction] from particular thicknesses of lead. The intensity of scattered primary gamma rays precluded a quantitative determination of the flux of 2.615-Mev gamma rays for values of the angle $\theta < 30^{\circ}$.

5.2 OAT Geometry III (Reflection of Neutrons)

Data on the reflection of neutrons, obtained for OAT Geometry III (see Fig. 8), are shown in Figures 30 through 35. Each figure contains a table in which are enumerated the parameters involved. The dots on each curve represent experimental data points.

The distributions of $T(h,y)$ are shown for h = 12 in. and h = 24 in. and represent measurements of the total radiation, incident plus reflected, for various values of y. The function $D(y)$ represents the distribution of radiation incident to the test materials. Thus, for a particular component of radiation, material, and material thickness, the distribution $R(h,y)$ of reflected radiation is given by

$$R(h,y) = T(h,y) - D(y).$$

A criterion for good geometry is that the total radiation for either slow or fast neutrons reflected from a particular thickness of material should be independent of h. To evaluate the geometry,

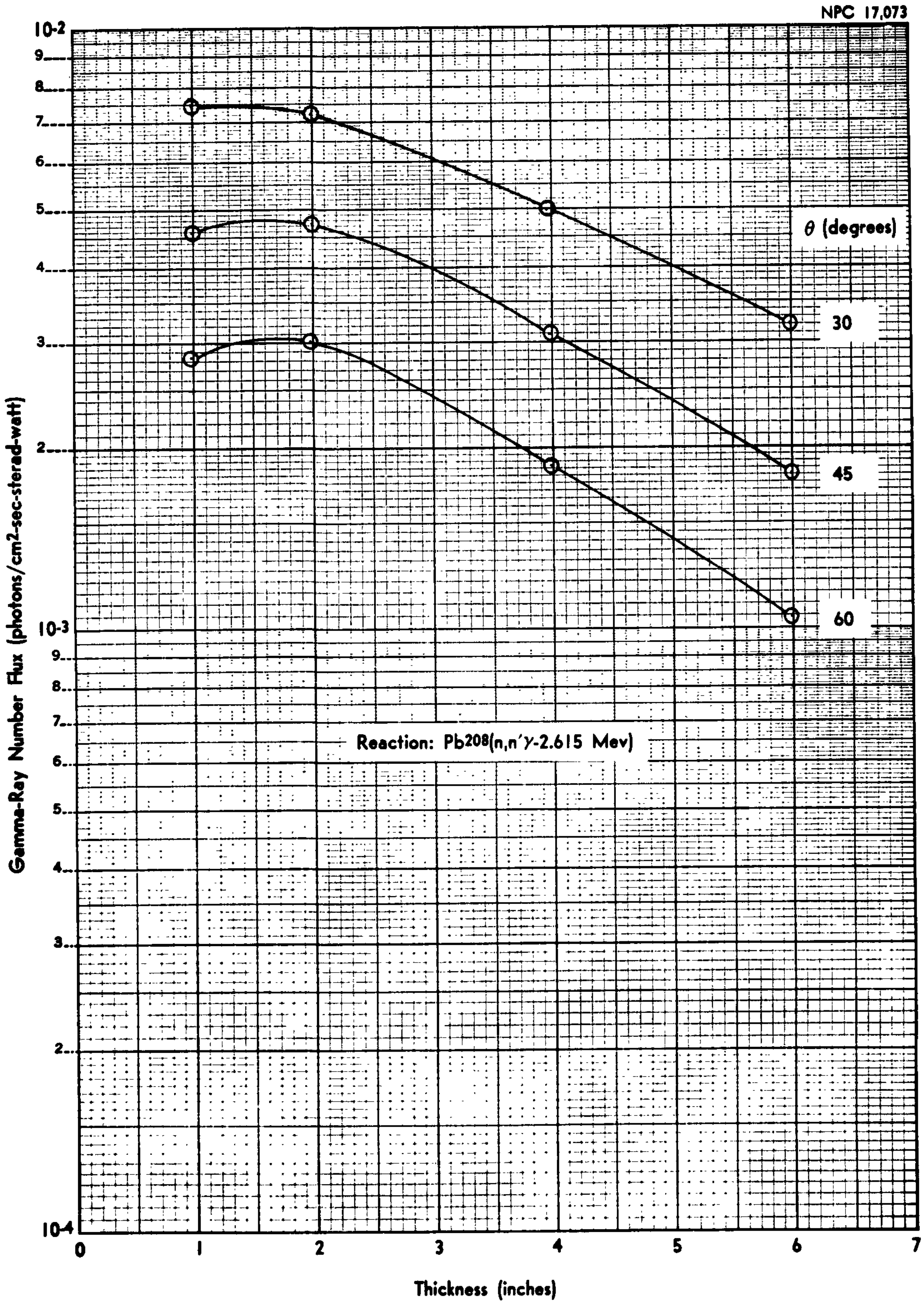


**Figure 29. Angular Distribution of Inelastically Produced Secondary Gamma Rays from Particular Thicknesses of Lead Slabs (R = 188 inches)**

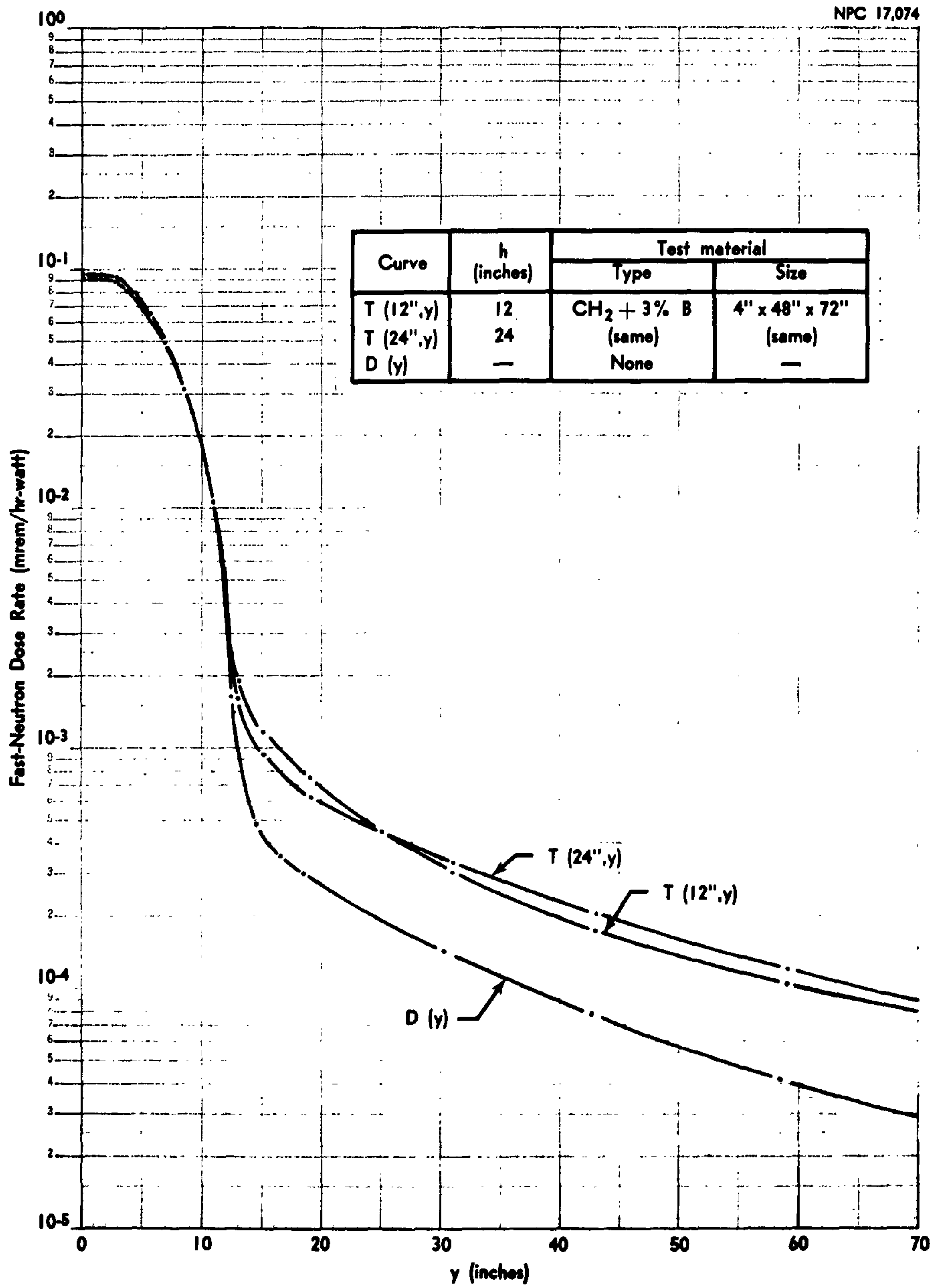


Figure 30. Reflection of Fast-Neutron Dose Rate from Borated Polyethylene

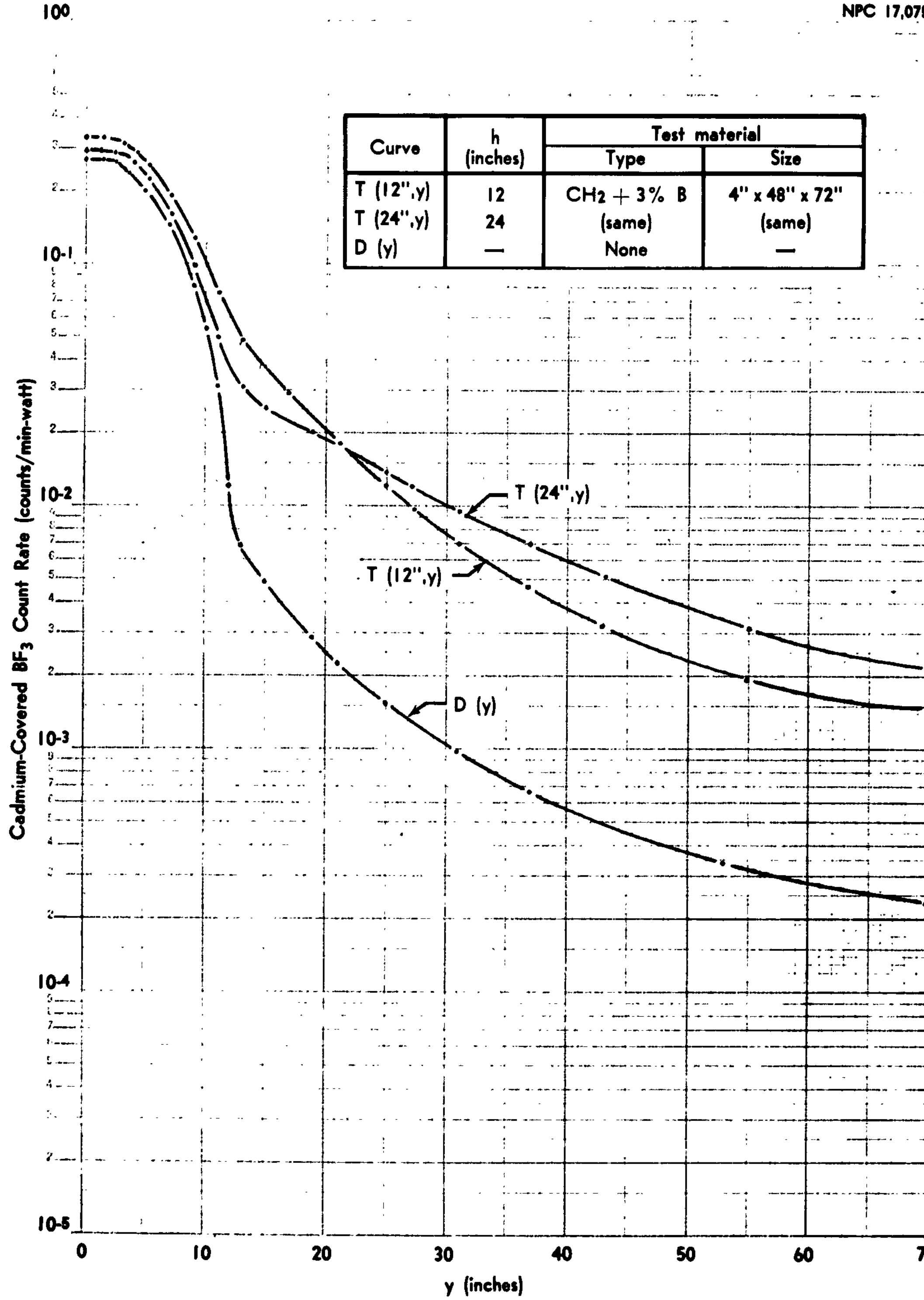


**Figure 31. Reflection of Relative Epithermal-Neutron Flux from Borated Polyethylene**

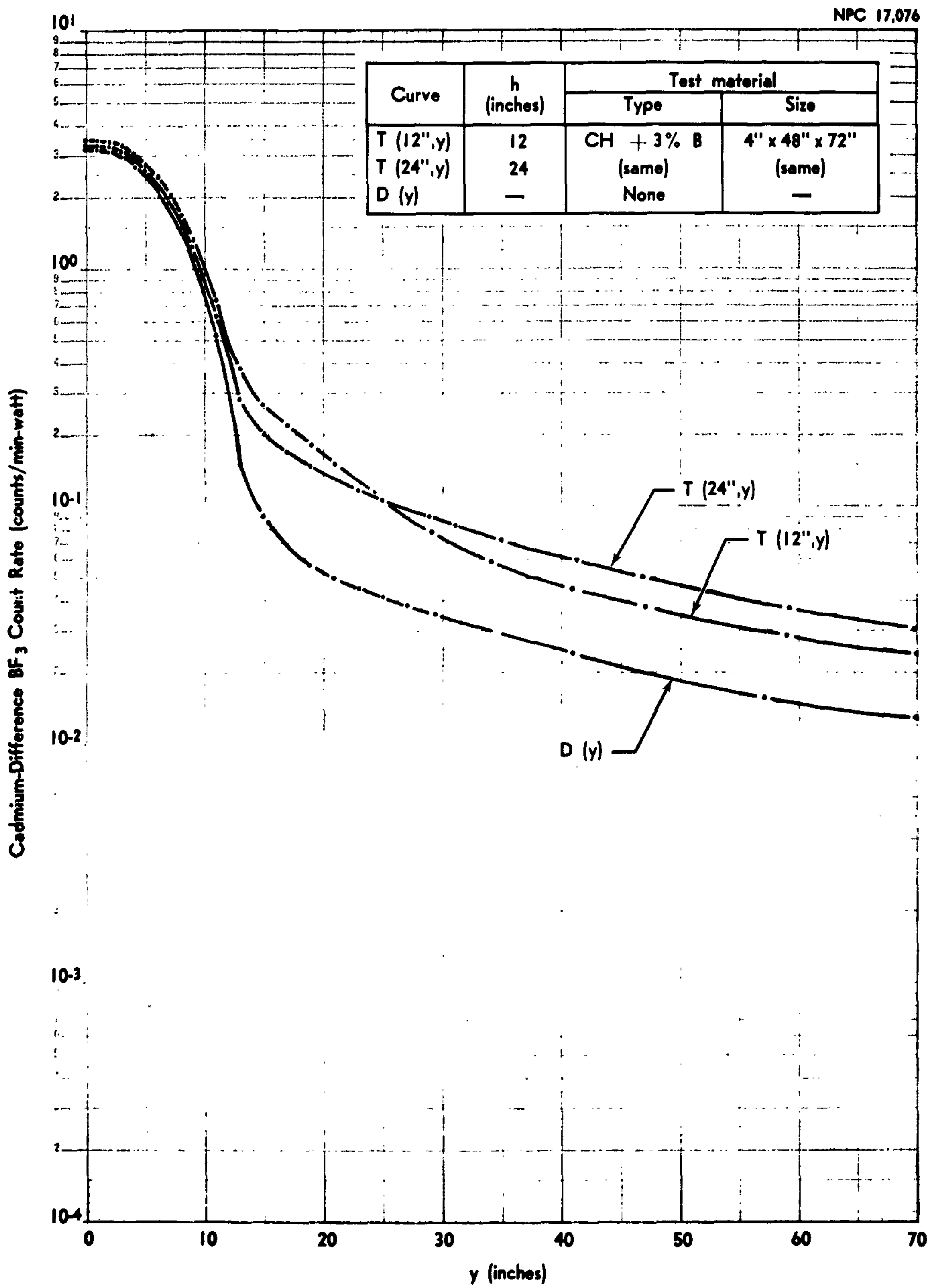


**Figure 32. Reflection of Relative Thermal-Neutron Flux from Borated Polyethylene**

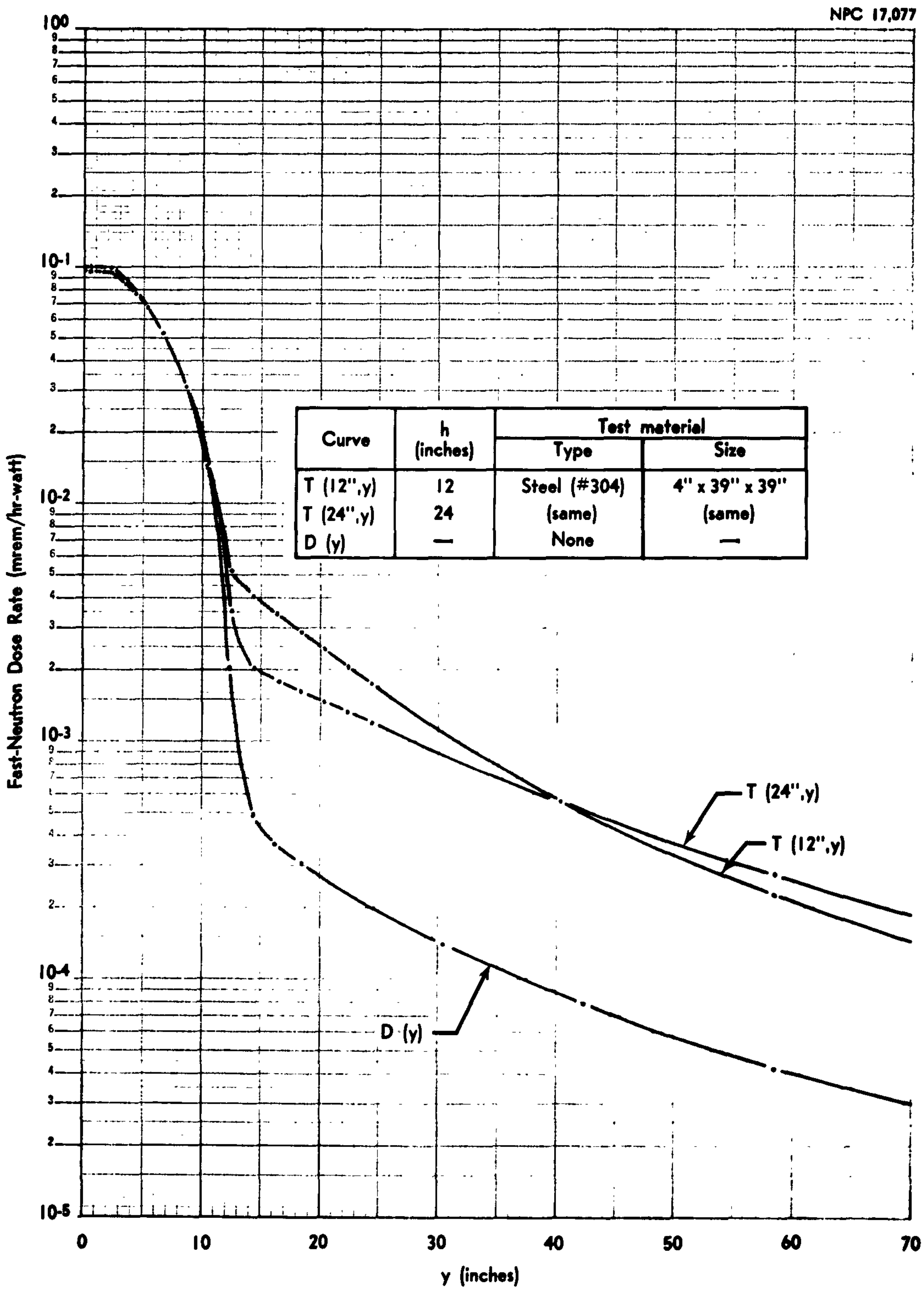


| Curve | h (inches) | Test material | |
|---|---|---|---|
| | | Type | Size |
| T (12",y) | 12 | Steel (#304) | 4" x 39" x 39" |
| T (24",y) | 24 | (same) | (same) |
| D (y) | — | None | — |

**Figure 33. Reflection of Fast-Neutron Dose Rate from Steel**

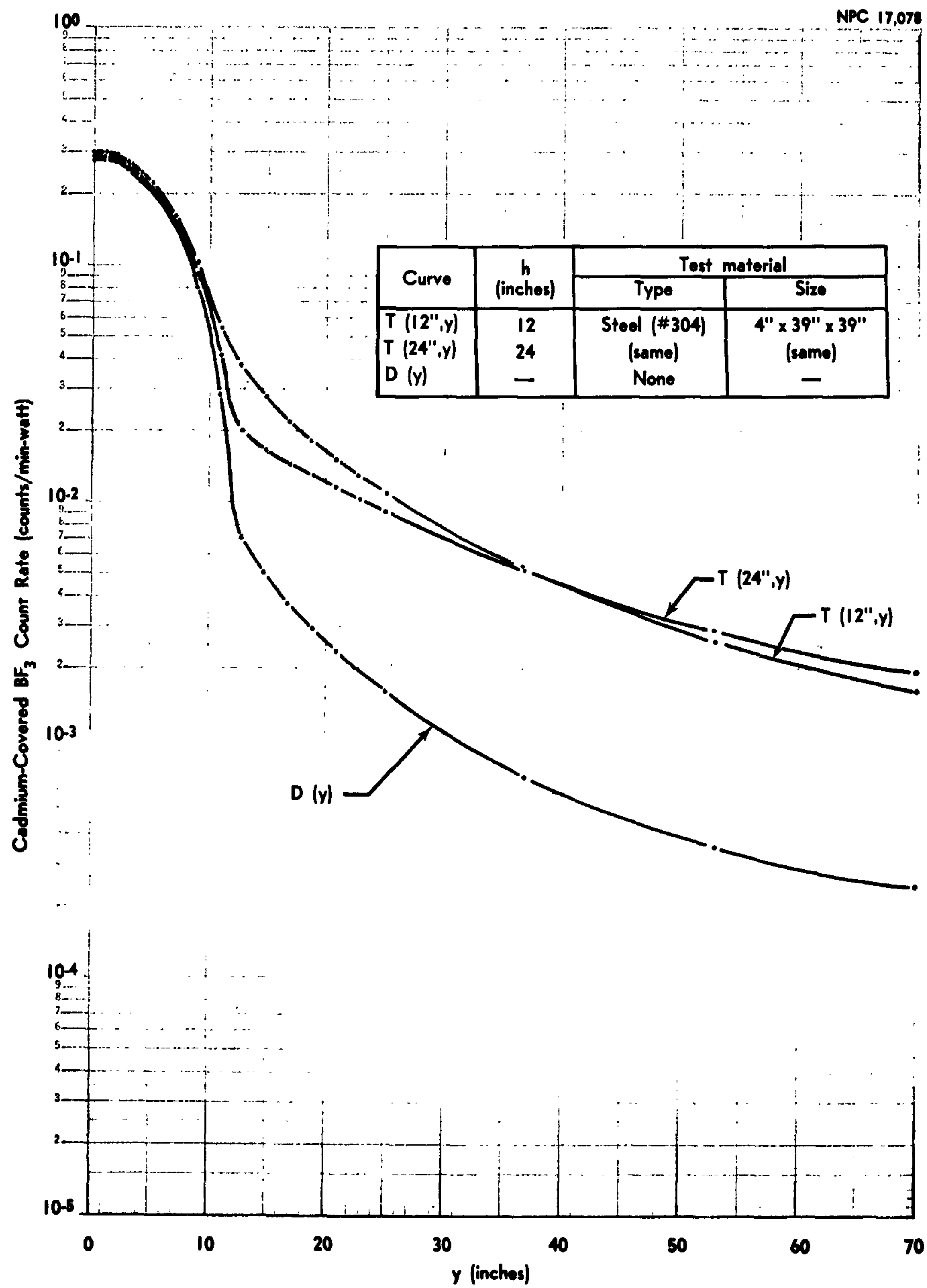


Figure 34. Reflection of Relative Epithermal-Neutron Flux from Steel

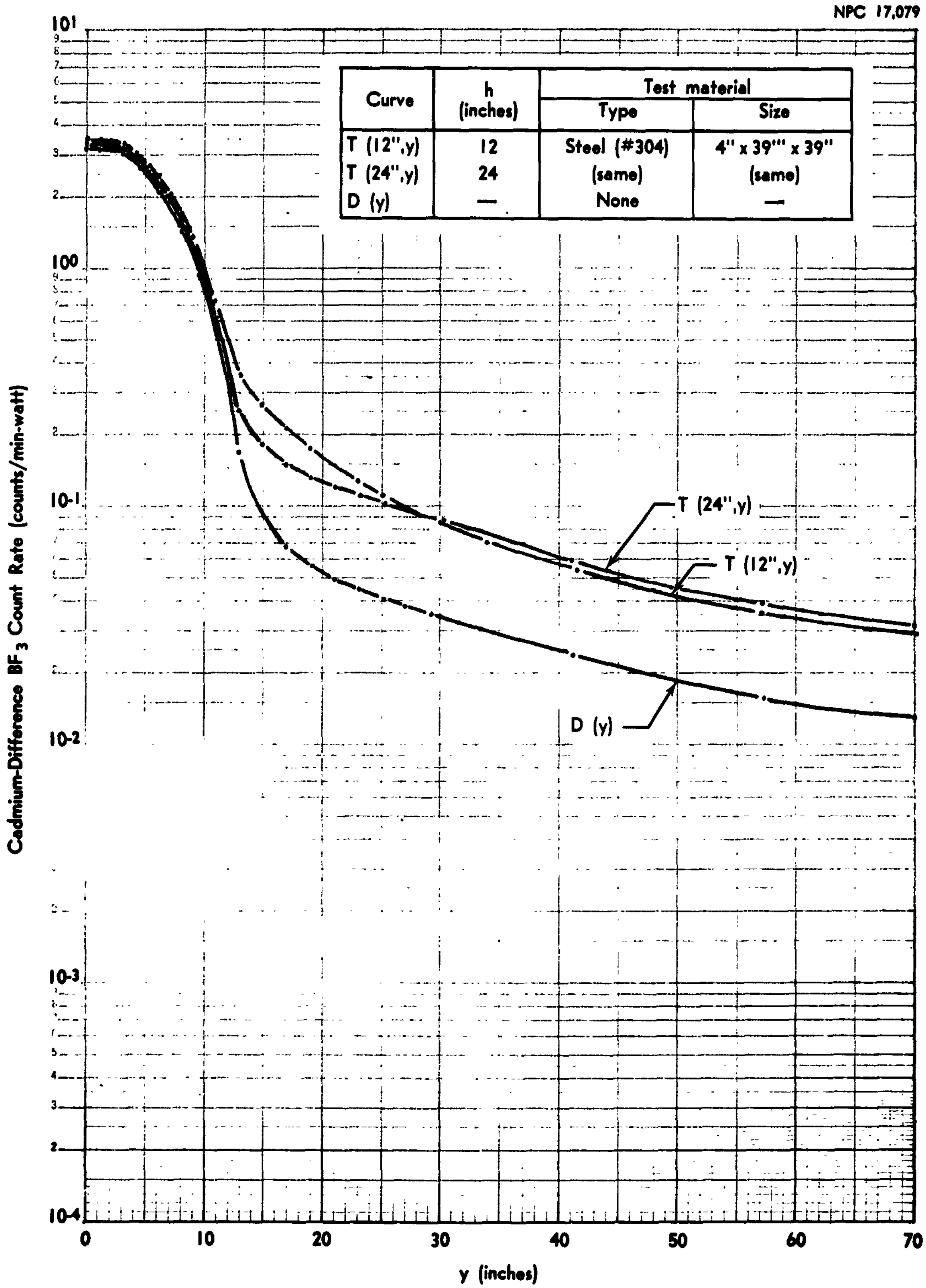


| Curve | h (inches) | Test material: Type | Test material: Size |
|---|---|---|---|
| T (12",y) | 12 | Steel (#304) | 4" x 39"' x 39" |
| T (24",y) | 24 | (same) | (same) |
| D (y) | — | None | — |

**Figure 35. Reflection of Relative Thermal-Neutron Flux from Steel**

$R(h,y)$ is expressed as $R(h,\phi)$ where, from Figure 8, $\phi$ is defined to be $\tan^{-1}(y/h)$. The condition for good geometry then requires the ratio $R_G$ to be equivalent to unity, where

$$R_G = \left[ \int_{\phi} R(12'',\phi)\ d\Omega \right] \left[ \int_{\phi} R(24'',\phi)\ d\Omega \right]^{-1} \tag{1}$$

and $d\Omega = 2\pi \sin \phi\ d\phi$.

The reflection coefficient $C_R$ is defined to be the ratio of reflected radiation to incident radiation. The ratio is expressed as

$$\bar{C}_r = \frac{1}{2} \left[ \int_{\phi} R(12'',\phi)\ d\Omega + \int_{\phi} R(24'',\phi)\ d\Omega \right] \left[ \int_{\beta} D(\beta)\ 2\pi\ \sin\beta d\beta \right]^{-1} \tag{2}$$

$D(y)$ is expressed as $D(\beta)$ with (see Fig. 8) $\beta = \tan^{-1}(y/135'')$. $\bar{C}_r$ denotes the fact that the average value of the reflected radiation measured at h = 12 in. and h = 24 in. is used in the foregoing equation.

By use of the data shown in Figures 30 through 35, $R_G$ and $\bar{C}_r$ - as defined by Equations 1 and 2 - were evaluated. Results of the evaluation are listed in Table 1. The proximity of $R_G$ to unity implies that the experimental geometry served the purpose for which it was intended. $\bar{C}_r$ values of 0.43 and 0.14 for steel and borated polyethylene, respectively, show that replacing steel with polyethylene reduced the reflected fast-neutron dose rate by a factor of 3.

For epithermal neutrons, the very large values of $\bar{C}_r$ denote the significance of incident fast neutrons slowing down within the test materials and then being reflected as epithermal neutrons. The value of $\bar{C}_r$ for thermal neutrons is, for the conditions under which data were obtained, independent of the test materials used.

Table 1

Geometry Evaluation and Reflection of Neutrons

| Type Data | Reflector Material* | $R_G$ | $\bar{C}_r$ |
|---|---|---|---|
| Fast-Neutron Dose Rate | $CH_2$ + 3% B | 1.00 | 0.14 |
| | Steel (#304) | 1.04 | 0.43 |
| Epithermal-Neutron Flux | $CH_2$ + 3% B | 1.01 | 1.47 |
| | Steel (#304) | 1.08 | 1.11 |
| Thermal-Neutron Flux | $CH_2$ + 3% B | 0.98 | 0.54 |
| | Steel (#304) | 1.03 | 0.56 |
| | Average | 1.02 | |

*All materials were 4 inches thick.

# VI. CONCLUSIONS AND RECOMMENDATIONS

This report, together with Volume II, presents a comprehensive collection of data that should prove valuable for evaluating calculational methods designed to predict the transport of radiation in a comparable geometry. Upon examination, the experimental data show that the geometries served the purpose for which they were intended, i.e., a well-defined narrow beam of neutrons and gamma rays was established and the undesirable components of radiation leakage and streaming were effectively suppressed. The data include (1) an accurate definition of the radiation source term, (2) information on the flux distribution of thermal and fast neutrons within the test materials, (3) the angular distribution of slow-neutron flux, fast-neutron and gamma-ray number-energy flux, and fast-neutron dose rate, and (4) the angular distribution of secondary gamma rays produced in and emerging from the test materials.

## 6.1 OAT Geometry I

### 6.1.1 Angular Distribution of Neutrons

The experimental data obtained on the angular distribution of neutrons provide information from which several conclusions and observations can be made. Of particular importance are the fast-neutron dose rate distributions for both polyethylene and lead (Figs. 13 and 14) and the epithermal-neutron flux distributions for borated polyethylene (Fig. 16). These distributions show the two distinct, and easily separable, scattered and uncollided contributions to the total distributions. These contributions are easily separable through material thicknesses of 15 and 6 inches of borated polyethylene and of lead, respectively. The foregoing indicates quite clearly that theoretical methods designed to predict the transport of radiation through slabs should treat the uncollided and scattered fluxes as two separate components.

A point of interest with regard to the polyethylene slabs is the small thickness of material required for the scattered component to reach equilibrium and develop its asymptotic shape; this is especially true for the fast- and epithermal-neutron fluxes. For lead, the asymptotic behavior of the fast-neutron scattered component is closely approximated (Fig. 14) at a slab thickness of 4 inches, whereas this condition for thermal-and epithermal neutrons is reached at a slab thickness nearer to 2 inches (Figs. 17 and 18). Also, for the thicknesses of lead investigated, it appears that the magnitude of the scattered component of thermal neutrons and of epithermal neutrons is very nearly independent of the material thickness.

6.1.2 Neutron Flux Distribution Within Test Materials

The distribution of neutron flux along the centerline of particular thicknesses of borated polyethylene and of lead slabs (Figs. 19 through 24) shows an expected exponential decrease in intensity for neutron energies greater than 6.3 Mev. A significant departure from exponential decay was not found for neutrons of energy greater than 2.9 Mev. These data provide information on the neutron number-energy flux as a function of depth into the material.

### 6.1.3 Secondary Gamma-Ray Production

The data shown in Figures 27, 28, and 29 pertaining to the production of secondary gamma rays in both a low-Z hydrogenous material and a high-Z material provide information which is of value for methods evaluation. The foregoing is particularly true for the 3% borated polyethylene in that a comparison of the flux distributions for the $H(n_{th}, \gamma\text{-}2.23$ Mev) and $C^{12}(n, n'\gamma\text{-}4.45$ Mev) reactions (Figs. 27 and 28) shows the large variation in relative intensities as a function of test material thickness and emission angle of the capture and inelastically produced gamma rays.

With respect to Figures 26 and 29 and previous investigations (Ref. 7) involving lead, the predominating secondary gamma-ray reaction is the $Pb^{208}(n, n'\gamma\text{-}2.62$ Mev) reaction. This gamma ray, being a "hard" gamma for penetration of high-Z materials, becomes more predominate with increasing lead thickness. Thus, for geometries utilizing lead as a shield material, a significant reduction in the secondary gamma-ray component, if the secondary gammas are important, can be effected by the use of radiolead, which is formed by removal of the $Pb^{208}$ isotope and costs approximately two and a half times more than chemically pure lead.

## 6.2 OAT Geometry III (Reflection of Neutrons)

In considering the results of the reflection measurements, it is again pointed out that the flux of fast neutrons incident to the test materials was greater than the thermal and epithermal neutron fluxes by factors of approximately 8 and 80, respectively.

Although only a 4-in.-thick slab each of 3% borated polyethylene and steel (type 304) were investigated, the data provide information from which several conclusions can be made.

With reference to Table 1, the reflection of fast neutrons from steel is a factor of 3 greater than reflection of fast neutrons from polyethylene. For slow neutrons, the ratio $\overline{C}_r$ includes both reflected slow neutrons and neutrons that emerge after being slowed down within the test material. Values of $\overline{C}_r$ greater than unity for epithermal neutrons emphasize the significant contribution from neutrons slowing down. The values of $\overline{C}_r$ for thermal neutrons are independent of the materials investigated.

Further investigations involving measurements of the transmission and reflection of radiation through and from shield materials as a function of material thicknesses and combinations of materials should provide valuable information for the design of shielded compartments. Reflection contributions from the cavity walls will increase the values shown in Table 1, which are for a single-slab geometry. Relative positions of hydrogenous and high-Z materials would considerably affect transmission, reflection, and secondary gamma-ray contributions to the total dose rate within a shielded compartment.

## REFERENCES*


1. Western, G. T., Energy and Angular Distribution Experiment. Volume II: Angular Distribution of Fast-Neutron and Gamma-Ray Number-Energy Flux. GD/FW Report FZK-9-183-2 (NARF-62-16T, to be published).

2. The 3-Mw Aircraft Shield Test Reactor. GD/FW Report FZK-9-161 (NARF-61-19R, August 1961).

3. An Investigation of the Characteristics of the Fast-Neutron Dosimeter. Convair-Fort Worth Report MR-N-50 (CVAC-262T, July 1954).

4. Johnson, C. F., $BF_3$ Thermal-Neutron Detection Channel. Convair-Fort Worth Report MR-N-47 (CVAC-263T, July 1954).

5. Warren, C. S., Nuclear Emulsion Techniques and Their Application for Measuring Fast-Neutron Energy Spectra. GD/FW Report FZK-9-159 (NARF-61-36T, March 1962).

6. Smith, F. W., and Mortensen, F. N., Calibration of the Anthracene Dosimeter. Convair-Fort Worth Report MR-N-30 (NARF-55-77T, October 1955).

7. Western, G. T., Experimental Determination of Neutron Flux Distributions in Slabs and of Emergent Secondary Gamma Rays. GD/FW Report FZK-9-176 (NARF-62-6T, June 1962).


*GD/FW reports published prior to July 1961 are referenced as Convair-Fort Worth reports.

DISTRIBUTION

FZK-9-183-1 31 December 1962

| Addressee | No. of Copies |
|---|---|
| ASRCNL | 2 |
| ASRCPR-2 | 2 |
| ASRMCE-1 | 2 |
| ASRMPE-2 | 2 |
| ASBMPT | 2 |
| ASTEN | 1 |
| ASAPRD-NS | 3 |
| GD/Convair | 1 |
| Convair-ASTRO | 2 |
| TIS | 20 |
| Lockheed-Ga. | 1 |
| Boeing AFPR | 1 |
| Douglas, Dept. A26 | 1 |
| North American | 1 |
| Pratt and Whitney | 1 |
| ORNL | 1 |
| NDA | 1 |
| Naval Ord Lab | 1 |
| Battelle-REIC | 1 |
| Air University Library | 1 |
| Radioplane | 1 |
| Republic Aviation | 1 |
| Vought-Aero | 1 |
| AFSWC (Tech Inf) | 1 |
| NASA-MSFC | 1 |
| NASA-Washington | 1 |
| AFPR-RCRFE | 1 |
| AFRDC-AE | 1 |
| ASRSMX-2 | 1 |
| ASRKMA | 2 |
| TRG | 1 |
| ASTIA | 10 |
| Sandia | 2 |
| Bureau of Ships | 1 |
| DOFL (Chief-230) | 1 |
| Aerojet-General Nucleonics | 1 |

UNCLASSIFIED

Nuclear Aerospace Research Facility, General Dynamics/Fort Worth, Fort Worth, Texas. ENERGY AND ANGULAR DISTRIBUTION EXPERIMENT. VOLUME I: ANGULAR DISTRIBUTION OF REACTOR RADIATION FROM SLABS AND OF EMERGENT SECONDARY GAMMA RAYS, by G. T. Western. 31 December 1962. 70 p. incl. illus., tables, 7 refs. (NARF-62-16T; FZK-9-183-1)
Contract AF(657)-7201 Unclassified report

Radiation from the Aerospace Systems Test Reactor positioned within the Outside ASTR Tank was directed with a narrow-beam slab geometry onto test materials of 3% borated polyethylene and of lead. Measurements for polyethylene and lead, except as noted, were made of (1) the radiation source term; (2) the flux distribution of thermal and fast neutrons within the test materials; (3) the angular distribution of thermal- and epithermal-neutron flux, fast-neutron dose rate, and secondary gamma rays from the test materials; (4) the reflection of neutrons from borated polyethylene and from steel; (5) the angular distribution of fast-neutron and gamma-ray number-energy flux; and (6) the angular distribution of gamma-ray dose rate resulting from primary gamma rays scattering in and from the test materials. Data for items 1, 2, 3, and 4 are presented in Volume I of this report; data for items 5 and 6 will be published in Volume II.

1. Neutron scattering, Gamma-ray spectra, Neutron activation, Neutron captive gamma rays, Neutron spectrum, Thermal neutrons, Fast neutrons, Inelastic scattering, Gamma-ray scattering, Dose rate, Neutron flux
2. Nuclear physics laboratories, Experimental data
3. Proportional counters, Nuclear spectroscopy, Pulse-height analyzers, Dosimeters, Gamma-ray spectroscopy, Scintillation counters, Nuclear radiation spectrometers, Neutron detectors, Crystal counters
4. Nuclear reactors
   I. G. T. Western
   II. Aeronautical Systems Division, Air Force Systems Command
   III. Contract AF(657)-7201

UNCLASSIFIED

UNCLASSIFIED

Nuclear Aerospace Research Facility, General Dynamics/Fort Worth, Forth Worth, Texas. ENERGY AND ANGULAR DISTRIBUTION EXPERIMENT. VOLUME I: ANGULAR DISTRIBUTION OF REACTOR RADIATION FROM SLABS AND OF EMERGENT SECONDARY GAMMA RAYS, by G. T. Western. 31 December 1962. 70 p. incl. illus., tables, 7 refs. (NARF-62-16T; FZK-9-183-1)
Contract AF(657)-7201 Unclassified report

Radiation from the Aerospace Systems Test Reactor positioned within the Outside ASTR Tank was directed with a narrow-beam slab geometry onto test materials of 3% borated polyethylene and of lead. Measurements for polyethylene and lead, except as noted, were made of (1) the radiation source term; (2) the flux distribution of thermal and fast neutrons within the test materials; (3) the angular distribution of thermal- and epithermal-neutron flux, fast-neutron dose rate, and secondary gamma rays from the test materials; (4) the reflection of neutrons from borated polyethylene and from steel; (5) the angular distribution of fast-neutron and gamma-ray number-energy flux; and (6) the angular distribution of gamma-ray dose rate resulting from primary gamma rays scattering in and from the test materials. Data for items 1, 2, 3, and 4 are presented in Volume I of this report; data for items 5 and 6 will be published in Volume II.

1. Neutron scattering, Gamma-ray spectra, Neutron activation, Neutron captive gamma rays, Neutron spectrum, Thermal neutrons, Fast neutrons, Inelastic scattering, Gamma-ray scattering, Dose rate, Neutron flux
2. Nuclear physics laboratories, Experimental data
3. Proportional counters, Nuclear spectroscopy, Pulse-height analyzers, Dosimeters, Gamma-ray spectroscopy, Scintillation counters, Nuclear radiation spectrometers, Neutron detectors, Crystal counters
4. Nuclear reactors
   I. G. T. Western
   II. Aeronautical Systems Division, Air Force Systems Command
   III. Contract AF(657)-7201

UNCLASSIFIED

UNCLASSIFIED

Nuclear Aerospace Research Facility, General Dynamics/Fort Worth, Fort Worth, Texas. ENERGY AND ANGULAR DISTRIBUTION EXPERIMENT. VOLUME I: ANGULAR DISTRIBUTION OF REACTOR RADIATION FROM SLABS AND OF EMERGENT SECONDARY GAMMA RAYS, by G. T. Western. 31 December 1962. 70 p. incl. illus., tables, 7 refs. (NARF-62-16T; FZK-9-183-1)
Contract AF(657)-7201 Unclassified report

Radiation from the Aerospace Systems Test Reactor positioned within the Outside ASTR Tank was directed with a narrow-beam slab geometry onto test materials of 3% borated polyethylene and of lead. Measurements for polyethylene and lead, except as noted, were made of (1) the radiation source term; (2) the flux distribution of thermal and fast neutrons within the test materials; (3) the angular distribution of thermal- and epithermal-neutron flux, fast-neutron dose rate, and secondary gamma rays from the test materials; (4) the reflection of neutrons from borated polyethylene and from steel; (5) the angular distribution of fast-neutron and gamma-ray number-energy flux; and (6) the angular distribution of gamma-ray dose rate resulting from primary gamma rays scattering in and from the test materials. Data for items 1, 2, 3, and 4 are presented in Volume I of this report; data for items 5 and 6 will be published in Volume II.

1. Neutron scattering, Gamma-ray spectra, Neutron activation, Neutron captive gamma rays, Neutron spectrum, Thermal neutrons, Fast neutrons, Inelastic scattering, Gamma-ray scattering, Dose rate, Neutron flux
2. Nuclear physics laboratories, Experimental data
3. Proportional counters, Nuclear spectroscopy, Pulse-height analyzers, Dosimeters, Gamma-ray spectroscopy, Scintillation counters, Nuclear radiation spectrometers, Neutron detectors, Crystal counters
4. Nuclear reactors

I. G. T. Western
II. Aeronautical Systems Division, Air Force Systems Command
III. Contract AF(657)-7201

UNCLASSIFIED

UNCLASSIFIED

Nuclear Aerospace Research Facility, General Dynamics/Fort Worth, Fort Worth, Texas. ENERGY AND ANGULAR DISTRIBUTION EXPERIMENT. VOLUME I: ANGULAR DISTRIBUTION OF REACTOR RADIATION FROM SLABS AND OF EMERGENT SECONDARY GAMMA RAYS, by G. T. Western. 31 December 1962. 70 p. incl. illus., tables, 7 refs. (NARF-62-16T; FZK-9-183-1)
Contract AF(657)-7201 Unclassified report

Radiation from the Aerospace Systems Test Reactor positioned within the Outside ASTR Tank was directed with a narrow-beam slab geometry onto test materials of 3% borated polyethylene and of lead. Measurements for polyethylene and lead, except as noted, were made of (1) the radiation source term; (2) the flux distribution of thermal and fast neutrons within the test materials; (3) the angular distribution of thermal- and epithermal-neutron flux, fast-neutron dose rate, and secondary gamma rays from the test materials; (4) the reflection of neutrons from borated polyethylene and from steel; (5) the angular distribution of fast-neutron and gamma-ray number-energy flux; and (6) the angular distribution of gamma-ray dose rate resulting from primary gamma rays scattering in and from the test materials. Data for items 1, 2, 3, and 4 are presented in Volume I of this report; data for items 5 and 6 will be published in Volume II.

1. Neutron scattering, Gamma-ray spectra, Neutron activation, Neutron captive gamma rays, Neutron spectrum, Thermal neutrons, Fast neutrons, Inelastic scattering, Gamma-ray scattering, Dose rate, Neutron flux
2. Nuclear physics laboratories, Experimental data
3. Proportional counters, Nuclear spectroscopy, Pulse-height analyzers, Dosimeters, Gamma-ray spectroscopy, Scintillation counters, Nuclear radiation spectrometers, Neutron detectors, Crystal counters
4. Nuclear reactors

I. G. T. Western
II. Aeronautical Systems Division, Air Force Systems Command
III. Contract AF(657)-7201

UNCLASSIFIED